FISEVIER

Contents lists available at ScienceDirect

# **Quaternary Science Reviews**

journal homepage: www.elsevier.com/locate/quascirev



#### Invited review

# Surface winds across eastern and midcontinental North America during the Last Glacial Maximum: A new data-model assessment



Jessica L. Conroy <sup>a, b, \*</sup>, Christina Karamperidou <sup>c</sup>, David A. Grimley <sup>d, a</sup>, William R. Guenthner <sup>a</sup>

- <sup>a</sup> Department of Geology, University of Illinois Urbana-Champaign, Urbana, IL, 61801, USA
- <sup>b</sup> Department of Plant Biology, University of Illinois Urbana-Champaign, Urbana, IL, 61801, USA
- <sup>c</sup> Department of Atmospheric Sciences, University of Hawaii at Mānoa, Honolulu, HI, 96822, USA
- <sup>d</sup> Illinois State Geological Survey, University of Illinois Urbana-Champaign, Champaign, IL, 61820, USA

#### ARTICLE INFO

#### Article history: Received 31 January 2019 Received in revised form 2 July 2019 Accepted 3 July 2019

Keywords: Loess Wind Last glacial maximum North America Climate model

#### ABSTRACT

Last Glacial Maximum (LGM) proxy evidence of surface wind direction across eastern and midcontinental North America comes primarily from loess and dune deposits, and overwhelmingly suggests surface winds had a strong westerly component. However, the season of sediment deposition and the temporal scale of wind information preserved in these deposits remains uncertain. Furthermore, paleoclimate model simulations over the last several decades have indicated a predominance of easterly winds across this region, due to the presence of an anticyclone over the Laurentide Ice Sheet as well as katabatic winds flowing off the ice sheet and over the adjacent land surface. Here we reassess model-data near-surface wind direction agreement using nine general circulation models participating in the LGM experiment of the third Paleoclimate Model Intercomparison Project (PMIP3) and a compilation of previously published paleowind directions from loess and dune deposits dating to the LGM. We find the highest overall modelproxy data agreement in winter (December-February), indicating predominantly westerly winds across the region in the LGM model simulations. We also find high zonal and meridional wind direction agreement in spring (March-May) and fall (September-November) in many models. Winter, spring and fall also have faster mean daily near-surface wind speeds in the LGM simulations relative to preindustrial control simulations. Thus, this model-data assessment suggests LGM aeolian deposition in the study region likely occurred dominantly in these three seasons, at times when local conditions favorable for aeolian deflation coincided with high wind speed events. Models that agree best with the proxy data have strengthened Aleutian and Icelandic Low pressure systems and a weakened Laurentide High pressure system, which constrains the spatial footprint of the Laurentide High to the ice sheet, reducing northeasterly winds near the ice sheet margin. A weaker Laurentide High in turn coincides with warmer surface temperatures over the ice sheet and the North Atlantic. The strength and location of semi-permanent pressure systems were thus key controls on surface wind direction across midcontinental and eastern North America during the LGM.

© 2019 Elsevier Ltd. All rights reserved.

#### 1. Introduction

Surface wind properties are associated with large-scale patterns of atmospheric circulation, including the orientation and strength of high and low semi-permanent pressure centers. Multimodel ensemble mean data from general circulation models (GCMs)

E-mail address: jconro@illinois.edu (J.L. Conroy).

participating in the fifth Coupled Model Intercomparison Project (CMIP5) indicate significant shifts in key aspects of global atmospheric circulation with increased greenhouse gas-driven radiative forcing. These include shifts in the strength and location of subtropical highs and the Aleutian Low, as well as a meridional migration of the mid-latitude jet streams (Scheff and Frierson, 2012; Barnes and Polvani, 2013; Yim et al., 2016; Gan et al., 2017). However, changes in surface wind characteristics with increased radiative forcing has been the subject of limited inquiry, partly due to limited model validation with observed surface wind speed data

<sup>\*</sup> Corresponding author. 1301 W Green St, Department of Geology, Urbana, IL, 61801. USA.

(Kulkarni and Huang, 2014; Kumar et al., 2015). Yet surface wind remains a variable of interest given the growth of wind-generated power in the midlatitudes and the associated impacts of wind strength on evaporation and atmospheric moisture balance (Roderick et al., 2007; St. George and Wolfe, 2009).

Surface wind information is frequently preserved in aeolian deposits and offers an opportunity to assess how wind patterns varied in the past with radically different radiative forcing and climate background states. Key examples are LGM loess and dune records from across the North American midcontinent and Atlantic Coastal Plain, which indicate predominantly westerly near-surface winds during the LGM (Muhs and Bettis, 2000; Mason et al., 2011; Markowich et al., 2015). However, a long-standing, model-paleoclimate proxy data discrepancy concerning the direction of LGM surface winds in this region extends back decades in the scientific literature. One of the first, atmosphere-only GCM simulations of LGM climate used by the Cooperative Holocene Mapping Project (COHMAP) group, who also conducted one of the first comprehensive paleoclimate data-model comparisons, suggested the presence of a strong near-surface anticyclone over the Laurentide Ice Sheet during the LGM (Kutzbach and Guetter, 1986; COHMAP, 1988). This anticyclone produced northeasterly surface winds on the eastern flank of the ice sheet and also south of the ice sheet margin, at odds with aeolian sedimentary evidence of predominantly westerly LGM surface winds in the midcontinental United States (Smith, 1942; Hallberg, 1979; Mason, 2001; Bettis et al., 2003).

Follow-up model-proxy data wind direction comparisons after the COHMAP investigation have continued to highlight this original model-proxy disagreement (Muhs and Bettis, 2000; Bromwich et al., 2005; Mason et al., 2011; Markewich et al., 2015), but have also suggested some potential avenues for resolution. Muhs and Bettis (2000) hypothesized that the passage of infrequent, eastward propagating cyclones, steered by the upper-level jet stream, led to near-surface silt entrainment and loess deposition downwind, even if mean wind direction was from the east, rather than the west. Thus, this manner of reconciliation stems from consideration of the temporal frequency of loess deposition (event-scale) versus climate model output of monthly, or monthly climatological, mean winds. Mason et al. (2011) show a westerly wind component west of 100°W in the original, January simulations interpreted by COHMAP, in agreement with wind direction inferred from aeolian deposits dating to the LGM in northeastern Colorado and the Nebraska Sand Hills region. This resolution considered more refined spatial patterns of surface winds, and also focused attention on the seasonality of aeolian deposition, as dominant wind direction varies seasonally, and the season of past aeolian deposition is often difficult to determine.

Subsequent LGM simulations using more advanced GCMs and regional climate models have not yet resolved this issue. For example, a higher resolution regional model (Polar MM5) continued to show easterly to northeasterly winds near the southern Laurentide Ice Sheet margin (Bromwich et al., 2004, 2005) where loess deposits clearly indicate westerly to northwesterly winds. Most recently, Markewich et al. (2015) summarized LGM wind directions in the Lower Mississippi Valley and the Atlantic Coastal Plain, highlighting the inability of previous LGM simulations (COHMAP, Polar MM5) to simulate aeolian observations of westerly to southwesterly winds in the South Atlantic Coastal Plain and west-northwesterly and northerly winds in the Middle Atlantic Coastal Plain. This discrepancy was also noted by previous researchers (Carver and Brook, 1989). However, a regional LGM simulation with another regional model, RegCM3, did suggest westerly winds over this region (Markewich et al., 2015).

Thus, model-proxy discrepancies in LGM surface wind direction

are not yet resolved. To date, no assessment of LGM model-proxy surface wind direction agreement has been conducted using the latest generation of comprehensive earth system models participating in PMIP3 (Braconnot et al., 2012). Such an approach, using multiple model simulations of the LGM that impose the same LGM boundary conditions, has the potential to lend greater insight into LGM atmospheric circulation and help resolve this decades-old model-proxy data mismatch. PMIP3 LGM model simulations have been previously used to compare proxies of LGM hydroclimate to simulated LGM upper-level wind, pressure, and precipitation patterns (Oster et al., 2015; Harrison et al., 2016; Lora, 2018; Wang et al., 2018), leading to new insights on key atmospheric circulation patterns, and their subsequent impacts on the terrestrial hydrologic budget. Here we assess the agreement between LGM surface wind directions from PMIP3 simulations and from sedimentary records of aeolian deposits across the midcontinent and the Atlantic Coastal Plain of North America. This analysis considers the degree of model-proxy agreement or disagreement with different GCMs, followed by an assessment of the role of large-scale circulation features in driving surface wind patterns. Our approach considers the seasonality of the proxy data, which impacts the degree of model-proxy agreement, and finally, the role of eventscale (i.e., daily) high wind speeds in producing LGM aeolian deposits.

#### 2. Methods

#### 2.1. Proxy data

As proxies for wind direction during the LGM, we consider paleowind direction inferred from loess thickness patterns, grain size, and geochemistry trends (with distance from deflation source), as well as sand dune orientations (Table 1). The thirty locations include sites stretching from eastern Colorado, across the Great Plains to the Midwest, and from the last glacial southern Laurentide Ice Sheet margin south to Mississippi and the southern to central Atlantic Coastal Plain (Fig. 1). Most of these sites were vetted and previously synthesized in LGM wind direction assessments by Muhs and Bettis (2000) and Markewich et al. (2015). The wind direction interpretations with respect to loess come from observations of the Peoria Silt (or Peoria Loess), a late Wisconsin Episode (last glacial) loess unit that is a surficial deposit over much of the midcontinental United States (Muhs and Bettis, 2000; Bettis et al., 2003). Areas with the thickest Peoria Loess occur along uplands proximal to major river valleys across the Midwest, thinning from west to east (Fig. 1). Loess deposits in the central Midwest, USA, have long been recognized as originating from the aeolian entrainment of the fine fraction of glacial meltwater deposits in major river valleys that drained the southern Laurentide Ice Sheet (Smith, 1942; Leighton and Willman, 1950). Dry, silt-sized deposits on the floodplains were periodically windswept into large dust clouds, which may have extended as much as 1 km above ground surface, based on modern observations (Crusius et al., 2011). Subsequent downwind deposition occurred extensively on vegetated uplands, where the silt was effectively trapped. A 'thinning' pattern, with decreases in loess thickness to the east or southeast of source valleys, is one of the key pieces of evidence of silt transport by westerly or northwesterly winds during the last glacial period (Smith, 1942; Fehrenbacher et al., 1965). Additionally, decreases in median grain size with distance from the source valley region and changes in geochemistry of loess (including major and minor trace elements, mineralogy, Pb isotope ratios, and U-Pb zircon ages) further help to pinpoint loess source regions, and thus support wind direction interpretations. Although the majority of last glacial loess deposits in the central Midwest (adjacent to the Missouri,

Table 1
LGM paleowind direction data used in this analysis. Map numbers refer to labels in Fig. 1. Coordinates are rounded to the nearest 0.5°. Site coordinates are determined from the original references. Wind directions in italics refer to evidence for minor winds for a given site. Data source abbreviations are LT: loess thickness, LP: loess particle size trends, LC: loess geochemistry trends, D: dune orientation, Dr: wind-aligned drainage in last glacial loess. For references, indicates original data source, indicates reference of work synthesizing data in a regional paleowind direction analysis. Of these 30 sites, 16 sites have meridional wind direction information, listed in the wind direction column. These 16 points are used to calculate the meridional model-data wind direction agreement in Fig. 6.

Map Number	Latitude (°N)	Longitude (°W)	Wind direction	Source	Reference <sup>1</sup>	Reference <sup>2</sup>	Unit/Age
1	39	83	W	LP	Rutledge et al. (1975)	Muhs and Bettis (2000)	Peoria Loess (29 - 16 ka)
2	39.5	84	W	LP	Rutledge et al. (1975)	Muhs and Bettis (2000)	Peoria Loess (29 - 16 ka)
3	39.5	82	W	LP	Rutledge et al. (1975)	Muhs and Bettis (2000)	Peoria Loess (29 - 16 ka)
4	38	88	NW (SW, E)	LT/LP	Fehrenbacher et al. (1965);	Muhs and Bettis (2000)	Peoria Loess (29 - 16 ka)
					Frazee et al. (1970)		
5	38.5	89.5	NW (SW)	LT/LP	Smith (1942);	Muhs and Bettis (2000)	Peoria Loess (29 - 16 ka)
				LT/LP	Frazee et al. (1970)		
6	39.5	89.5	NW (SW)	LT/LP	Smith (1942);	Muhs and Bettis (2000)	Peoria Loess (29 - 16 ka)
				LT/LP	Frazee et al. (1970)		
7	36.5	89.5	W	LT	Rodbell et al. (1997)	Muhs and Bettis (2000)	Peoria Loess (19 $\pm$ 4 ka)
8	35.5	90	W	LT	Rodbell et al. (1997)	Muhs and Bettis (2000)	Peoria Loess (23 $\pm$ 2 ka)
9	42.5	91	W	LT/LP	Leigh and Knox (1994)	Muhs and Bettis (2000)	Peoria Loess (29 - 16 ka)
10	43.5	91.5	W	LP	Mason et al. (1994)	Muhs and Bettis (2000)	Peoria Loess (29 - 16 ka)
11	42	92	NW	Dr	Hallberg (1979)	Muhs and Bettis (2000)	Peoria Loess (29 - 16 ka)
12	39	92.5	W	LT/LC	Ebens and Connor (1980)	Muhs and Bettis (2000)	Peoria Loess (29 - 16 ka)
13	39.5	94	W	LT/LC	Ebens and Connor (1980)	Muhs and Bettis (2000)	Peoria Loess (29 - 16 ka)
14	40.5	95.5	W	LT/LC	Ebens and Connor (1980)	Muhs and Bettis (2000)	Peoria Loess (29 - 16 ka)
15	42	95.5	NW	Dr	Hallberg (1979)	Muhs and Bettis (2000)	Peoria Loess (29 - 16 ka)
16	41.5	96	W	LP/LC	Muhs and Bettis (2000)	Muhs and Bettis (2000)	Peoria Loess (29 - 16 ka)
17	41	96	W	LT/LP	Ruhe (1954)	Muhs and Bettis (2000)	Peoria Loess (29 - 16 ka)
18	41	98	NW	LT/LC	Mason (2001);		Peoria Loess (29 - 16 ka)
					Aleinikoff et al. (2008)		
19	41.5	100	NW	D	Mason et al. (2011)		25 - 15 ka
20	40	101	NW	LP	Swineford and Frye (1951)	Muhs and Bettis (2000)	Peoria Loess (29 - 16 ka)
21	40	103	NW	LP/LC	Aleinikoff et al. (1999);	Muhs and Bettis (2000)	Peoria Loess (24 - 14 ka)
					Muhs et al. (1999)		
22	32.5	91	NW	LP	Matalucci et al. (1969);	Muhs and Bettis (2000)	Peoria Loess (29 - 16 ka)
					Snowden and Priddy (1968)		
23	30.5	86	SW and SE	D	Otvos (2004)	Markewich et al. (2015)	31 - 24 ka
24	30	84.5	SW and SE	D	Otvos (2004)	Markewich et al. (2015)	31 - 22 ka
25	31.5	84	W	D	Ivester et al. (2001);	Markewich et al. (2015)	30 - 15 ka
					Ivester and Leigh (2003)		
26	32	82	W	D	Ivester et al. (2001);	Markewich et al. (2015)	30 - 15 ka
					Ivester and Leigh (2003)		
27	32.5	82	SW	D	Carver and Brook (1989)	Markewich et al. (2015)	~30 - 15 ka
28	33.5	79	SW	D	Carver and Brook (1989)	Markewich et al. (2015)	~30 - 15 ka
29	34.5	78.5	SW	D	Carver and Brook (1989)	Markewich et al. (2015)	~30 - 15 ka
30	38.5	75.5	NW	D	Carver and Brook (1989)	Markewich et al. (2015)	~30 - 15 ka

Mississippi, Illinois, Wabash, and Ohio River valleys) are derived from glacial meltwater sediments, some last glacial loess in the Great Plains is derived from nonglaciogenic sources (Aleinikoff et al., 2008). In these instances, loess geochemistry plays a more critical role in defining source regions and the pathway from sediment source to sink.

Dunes provide supplemental information on past wind, with the orientation of sand dunes preserving a record of the wind direction. There are fewer sites with last glacial dune information for our study region (Table 1), but the existing records support loess-based wind interpretations when they are located in loess-covered regions. In the Atlantic Coastal Plain, where loess is limited or absent, dune orientation is the main indicator of late glacial wind direction (Markewich et al., 2015).

In terms of chronology, the Peoria Loess has been benchmarked to the late Wisconsin Episode, or last glacial period. Broadly, it is defined as spanning an age range of 30 to 14 ka (Bettis et al., 2003; Muhs, 2013). Most of the earliest loess research predated numerical dating techniques, but early radiocarbon measurements from Peoria Loess (Frye et al., 1968; Snowden and Priddy, 1968) and subsequent chronologic investigations, using both radiocarbon and luminescence techniques, support this age range (e.g., Rodbell et al., 1997; Forman and Pierson, 2002; Bettis et al., 2003; Muhs et al.,

2013; Pigati et al., 2015; Nash et al., 2018). The age span of the Peoria Loess extends through the LGM, including several thousand years before and after 21 ka, the year specifically prescribed in the model simulations (Table 1). However, although the last glacial loess and dunes span a larger age range than the model simulations, the inferred wind directions remain consistent throughout these late glacial sedimentary packages, allowing us to compare the 21 ka model simulations and the proxy wind information, as has been done in previous investigations into this problem.

Regarding LGM proxy coordinates, we use the site locations given in the original references, rather than the vectors plotted in past syntheses, as multiple sites in a region were often averaged together into a single vector in earlier studies. With higher spatial resolution climate models now available, we define individual sites if they are separated by a distance greater than  $0.5^{\circ}$  latitude or  $0.5^{\circ}$  longitude. Although the meridional component of the paleowind direction in loess deposits could be biased due to the spatial orientation of sampling schemes (Muhs and Bettis, 2000), we separately assess the zonal (u, N = 30) and meridional (v, N = 16) components of inferred surface wind direction when meridional wind direction information is available. We also note where authors provide evidence for minor, secondary wind directions and discuss the implications of evidence for multiple wind directions.

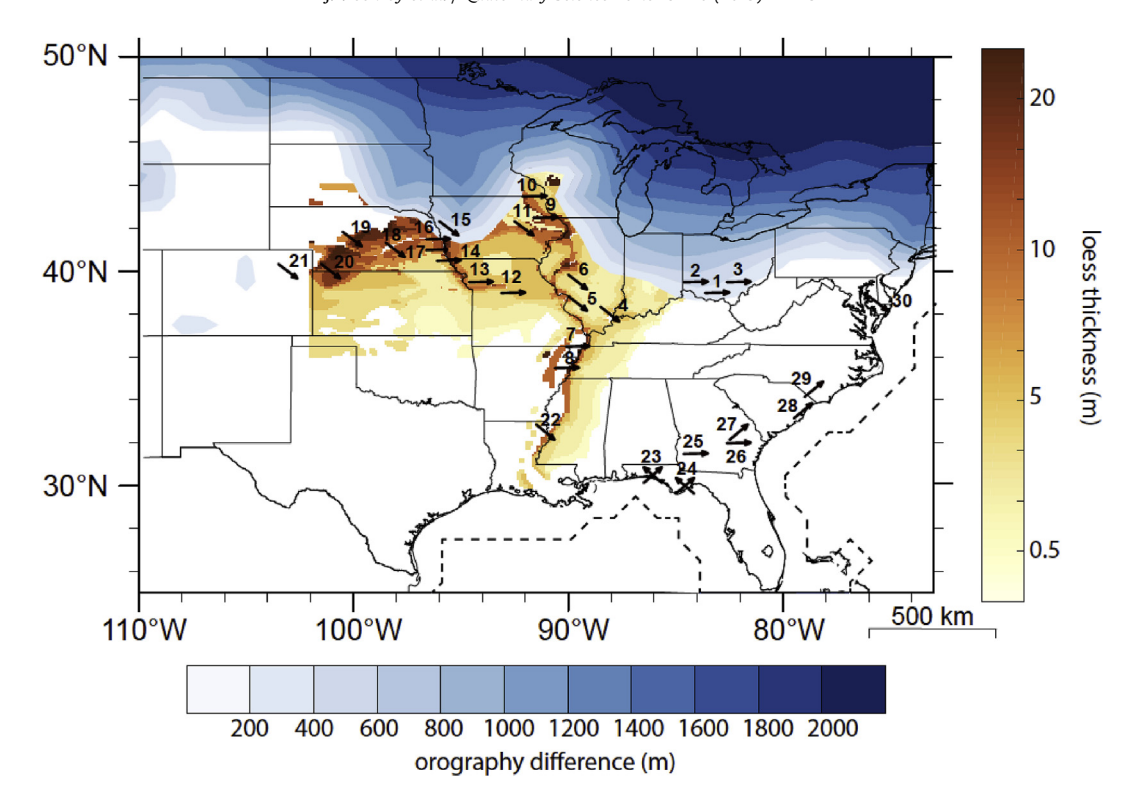


Fig. 1. Map indicating study region. Blue colored contours indicate the margin and elevation of the PMIP3 21 ka Laurentide Ice Sheet, as designated by the difference between LGM and pre-industrial control orography (m). Yellow-orange shading denotes thickness of midcontinental Peoria loess from the Kohfeld and Muhs (2001) dataset. Numbered vectors indicate locations of proxy surface wind direction data. For references and information corresponding to numbers, please see Table 1. LGM land margin indicated by dashed line. Modern political boundaries, geophysical features, and scale for 40°N provided for visual reference.

Table 2
PMIP3/CMIP5 model simulations used in this analysis. Variable acronyms are designated by CMIP5 and include zonal (ua) and meridional (va) winds at different pressure levels in the atmosphere, and at the surface (uas, vas), sea level pressure (psl), surface air temperature (tas), and mean daily surface wind speed (sfcWind\_day). \*Two different experiments are considered with different ice sheet configurations. p150 uses the Ice-5G ice sheet (Peltier, 2004), and p151 uses a lower elevation ice sheet (Licciardi et al., 1998).

Institution	Model name	Experiments	Resolution (lat x lon)	Variables
National Center for Atmospheric Research	CCSM4	LGM, piControl	$0.94^{\circ} \times 1.25^{\circ}$	ua, va, psl, sfcWind_day, tas
Centre National de Recherches Météorologiques/Centre Européen de	CNRM-	LGM, piControl	$1.4^{\circ} \times 1.4^{\circ}$	ua, va, uas, vas, psl, tas
Recherche et de Formation Avancée en Calcul Scientifique	CM5			
Alfred Wegener Institute	COSMOS- ASO	LGM, piControl	$3.71^{\circ} \times 3.75^{\circ}$	ua, va, uas, vas, psl, sfcWind_day, tas
Institute of Atmospheric Physics, Chinese Academy of Sciences, and Tsinghua University	FGOALS- g2	LGM, piControl	$2.8^{\circ} \times 2.8^{\circ}$	ua, va, psl, tas
NASA Goddard Institute for Space Studies	GISS-E2- R	LGM: p150 and p151*, piControl	$2.0^{\circ} \times 2.5^{\circ}$	ua, va, uas, vas, psl, tas
L'Institut Pierre-Simon Laplace	IPSL- CM5A-LR	LGM, piControl	$1.87^{\circ} \times 3.75^{\circ}$	ua, va, uas, vas, psl, tas
Japan Agency for Marine-Earth Science and Technology, Atmosphere and Ocean Research Institute (The University of Tokyo), National Institute for Environmental Studies	MIROC- ESM	LGM, piControl	$2.8^{\circ} \times 2.8^{\circ}$	ua, va, uas, vas, psl, sfcWind_day, tas
Max Planck Institute for Meteorology	MPI- ESM-P	LGM, piControl	$1.87^{\circ}\times1.87^{\circ}$	ua, va, uas, vas, psl, sfcWind_day, tas
Meteorological Research Institute	MRI- CGCM3	LGM, piControl	$1.12^{\circ} \times 1.12^{\circ}$	ua, va, uas, vas, psl, sfcWind_day, tas

## 2.2. Model data

The PMIP3 simulations, which include the LGM simulations assessed here, as well as mid-Holocene and last millennium simulations, have been used to evaluate many of the same models used to project future climate change in the Working Group 1 report to the Intergovernmental Panel on Climate Change (Flato et al., 2013).

The PMIP3 LGM simulations include equilibrium simulations from nine different comprehensive global earth system models (Table 2). These models are all coupled, and include atmosphere, ocean, land, sea ice, and in some cases, dynamic vegetation models. The LGM simulations are all forced with the same boundary conditions in order to approximate climate 21 ka before present. Key forcing factors include ice sheet extent and topography, atmospheric

greenhouse gas concentrations, land-sea mask, land surface, and orbital configurations (Braconnot et al., 2012; Harrison et al., 2016). Some LGM forcing factors that are likely important are missing, notably dust loading and vetted differences in spatial vegetation distributions (Harrison et al., 2016). However, despite these uncertainties, the set-up of PMIP3 is advantageous for diagnosing model performance relative to paleoclimate observations, given all imposed forcing factors are the same across the suite of models participating in the experiment. An inherent assumption in this intercomparison exercise is that consistent agreement across models and between model output and paleo-data is the result of realistic and correct mechanisms at work in the climate system (Braconnot et al., 2012).

Despite the uniform boundary conditions, the imposed ice sheet varies with model spatial resolution, and as a result the ice sheet margin varies from model to model (see Supplemental Fig. 1 for complete view of Laurentide orography differences across models). Although substantially improved over earlier iterations, these ice sheet margins, as expressed with orography differences between the LGM and pre-industrial control, do not completely align with geologic evidence of maximum LGM ice sheet extent. For example, the PMIP3 designated ice sheet (assessed as orography difference) extends too far into Ohio, and Pennsylvania and the Des Moines glacial lobe is shifted ~100 km west of its mapped maximal extent in north-central Iowa (e.g., Fig. 1). In addition, two different archived LGM experiments for the GISS-E2-R model have different ice sheet configurations (p150 and p151). Simulation p150 uses the Ice-5G model (Peltier, 2004), which has a higher elevation area west of Hudson Bay, and p151 uses a lower elevation ice sheet (Licciardi et al., 1998), with three areas of highest elevation to the west, south, and east of Hudson Bay (Supplemental Fig. 1). The PMIP3 designated ice sheet is a blend of three different ice sheet reconstructions, and ultimately falls between the two extremes simulated by GISS-E2-R (Ullman et al., 2014). In the following sections, we compare both the GISS-E2-R p150 and p151 simulations to the other PMIP3 models. All PMIP3 data used in this analysis are archived and available to the public via the Earth System Grid Federation (https://www.earthsystemgrid.org/).

We assess zonal and meridional surface wind direction (variables *uas* and *vas*, Table 2). We also assess LGM data relative to preindustrial control (piControl) data, or data from non-evolving, equilibrium simulations with modern forcing prior to the emission of anthropogenic greenhouse gases and large-scale anthropogenic land use change. In the FGOALS and CCSM4 models, surface wind was not archived, so we consider wind direction at 925 mb, the closest approximation to the surface, relative to land elevation (variables *ua*, *va* at 925 mb). The high elevation site in Colorado (site 21) only has model wind speed data at the 700 mb level in CCSM4. Similarly, in FGOALS, the few higher elevation sites only have wind speed data where the surface intersects the 850 mb or 700 mb level. Thus, we assess available model wind direction at these levels in our analysis for those higher elevation sites (Supplemental Figs. 2–3).

## 2.3. Model and data analyses

We consider boreal winter, spring, summer, and fall zonal and meridional wind directions (DJF, MAM, JJA, SON), taken from the archived LGM and piControl monthly climatology of each model using the National Center for Atmospheric Research (NCAR) Command Language (NCL, 2018). For the gridded coordinates closest to each proxy data point, we test whether the zonal wind direction is westerly or easterly and whether the meridional direction (when available) is northerly or southerly in the models versus the data. (Figs. 2–5, Supplemental Figs. 4–7). We do not assess LGM wind

direction as anomalies relative to the pre-industrial control wind direction because aeolian archives record actual wind direction, not anomalies; thus, comparisons of proxy-inferred wind direction to model wind direction anomalies are potentially misleading. For example, an easterly anomaly could represent weaker westerly winds or easterly winds. Rather than just considering the total agreement of proxy and model wind directions at the sites as a percentage, we also account for agreement by chance using Gwet's AC1 (Gwet, 2002). This agreement index summarizes the percent agreement between each model and the proxy data, while also accounting for chance agreement. The calculation is based on a tabular organization of the instances of agreement and disagreement (Table 3).

Gwet's AC1 value is calculated as:

$$AC1 = \frac{p - e(\gamma)}{1 - e(\gamma)} \tag{1}$$

where the variable p is

$$p = (A+D)/N \tag{2}$$

and

$$e(\gamma) = 2P_1 \ (1 - P_1) \tag{3}$$

where

$$P_1 = \frac{(A1 + B1)/2}{N} \tag{4}$$

Gwet's AC1 values range from -1 to 1 (Fig. 6). A value of 1 indicates perfect agreement, with model wind direction at each site agreeing with proxy zonal wind direction at each site, and 0 indicates no agreement greater than agreement by chance. Complete opposite wind directions (i.e., model winds are all easterly and proxy winds are all westerly) is indicated by -1. We calculate Gwet's AC1 for each model-data pair, considering each wind direction (meridional and zonal) in each season separately.

Following our comparison of zonal and meridional surface wind direction in the model simulations and the proxies, we assess sea level pressure (variable psl, henceforth abbreviated as SLP in the text), wind speed, and wind direction at 925 mb and 200 mb in the models that have the three highest and lowest AC1 scores with the proxy data (Table 4, Figs. 7 and 8, Supplemental Fig. 8). We also assess zonal wind speed and direction variations with height in a latitude versus height map of zonal wind speeds averaged over 90°W-100°W (Fig. 9). We then perform a similar analysis with surface air temperature (variable tas, Fig. 10). We calculate multimodel mean values for these variables and plot the differences in the multimodel means of the top and bottom-ranking models. For near-surface wind speed and direction in Fig. 8 we use 925 mb winds rather than surface winds, given that two of the models do not have surface winds archived. In areas where the 925 mb pressure level is below the corresponding surface pressure, we extrapolate by solving Poisson's equation with an iterative relaxation scheme; this is performed with function poisson\_grid\_fill in NCAR Command Language (NCL, 2018). In our exploration of model bias in the discussion, we also assess wind speed and direction from 700 to 925 mb (Supplemental Fig. 10). Finally, for five models where LGM daily wind speeds have been archived (Table 2, variable sfcWind\_Day), we assess the frequency of high wind speed (>8 m/s) in the LGM and pre-industrial controls runs (Fig. 11). We assess the seasonal frequency of mean daily wind speeds greater than 8 m/s in the core region of our study area, from 30°N to 40°N, 100°W-92°W, south of the ice sheet and excluding open ocean grid points.

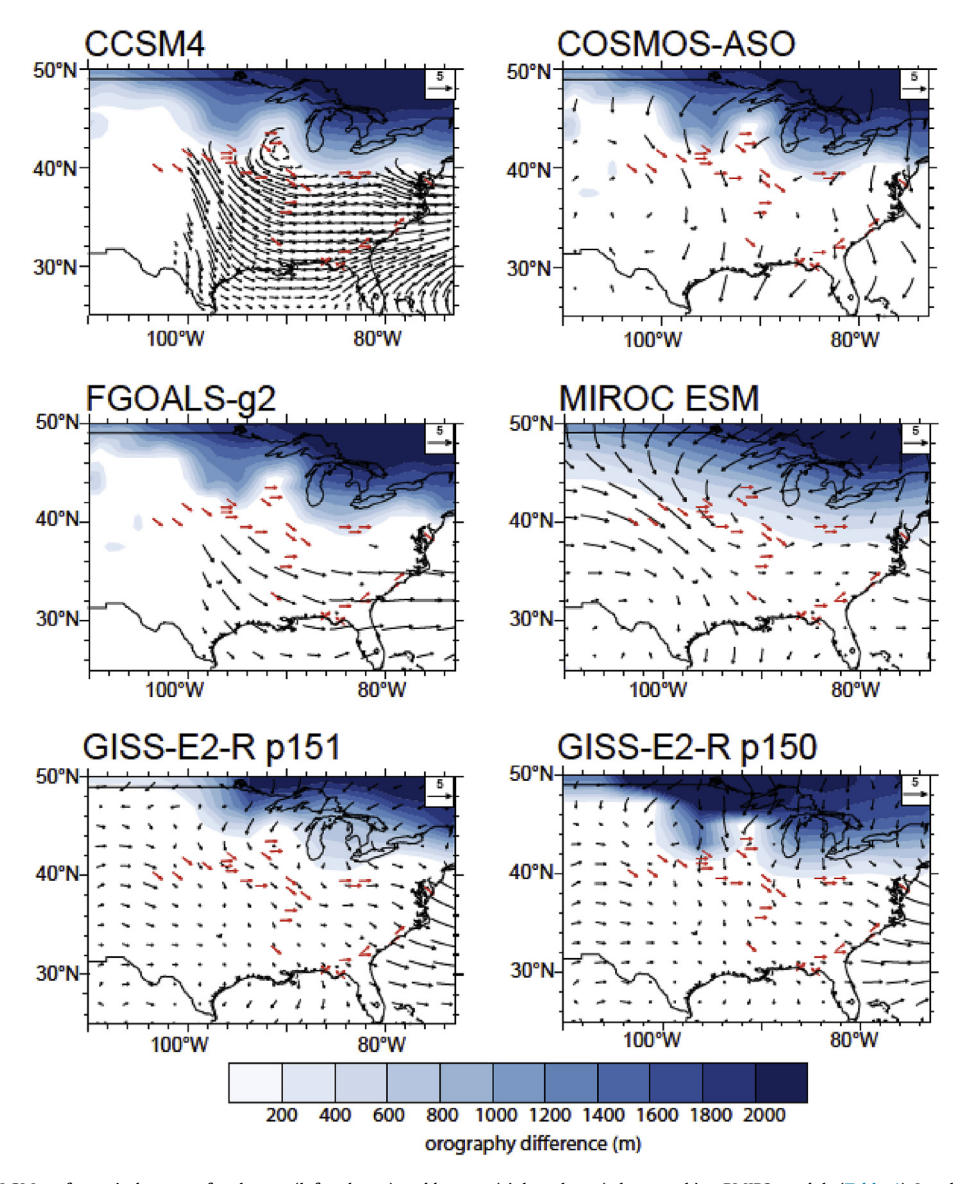


Fig. 2. Boreal winter (DJF) LGM surface wind vectors for the top (left column) and bottom (right column) three ranking PMIP3 models (Table 4). Ice sheet elevation shown in blue. Paleovectors are in red. FGOALS and CCSM4 do not archive near surface winds or winds at geopotential heights below the actual land surface, so 925 mb winds are plotted. Please refer to Supplemental Figs. 2 and 3 for 850 mb and 700 mb winds in CCSM4 and FGOALS, and Supplemental Fig. 4 for comparison of DJF pre-industrial control and LGM winds for all models.

#### 3. Results

Wind direction preserved in spatial patterns of LGM loess thickness, grain size, and geochemistry, as well as dune orientations, suggest the dominant zonal wind direction was westerly at nearly every proxy site (Fig. 1). Overall, the dominant LGM wind direction in the midcontinent was northwesterly or westerly, whereas wind direction on the Atlantic Coastal Plain was northwesterly on the Delmarva Peninsula and southwesterly along the southern Atlantic Coastal Plain (Carver and Brook, 1989). There is also evidence of variable wind directions preserved in loess thickness patterns, dunes, and other geomorphologic features at certain locations (Smith, 1942; Fehrenbacher et al., 1965; Handy, 1976; Hallberg, 1979; Muhs et al., 2001). In this synthesis, the two LGMdated dune sites in northwestern Florida indicate zonal winds from both the southwest and southeast (Otvos. 2004), and secondary easterly winds have been interpreted from last glacial loess records in Illinois and Indiana (Smith, 1942; Fehrenbacher et al., 1965).

The prevailing winter LGM winds in the model simulations are largely westerly, but many models have a more northerly or northeasterly component over the ice sheet and near the ice sheet margin (Fig. 2, Supplemental Fig. 4). Easterly winds also occur over or near the Gulf of Mexico (similar to the pre-industrial control). The winter meridional wind direction is largely northerly in most LGM model simulations, even over the Gulf of Mexico. Only CCSM4 has southerly winds in winter, which are limited to the southern Atlantic Coastal Plain. In the higher resolution CCSM4 and CNRM models, a small, distinctive, anti-cyclonic circulation feature is also present at the ice-land boundary in vicinity of the Driftless Area, centered at 42°N, 90°W.

Spring, summer, and fall winds in the nine LGM model simulations are weaker in strength relative to winter, with more instances of easterly winds at the proxy sites (Figs. 3–5, Supplemental Figs. 5–7). However, some models, such as FGOALS, still show predominantly westerly winds, even in summer. Summer meridional flow into the midcontinent is typically southerly,

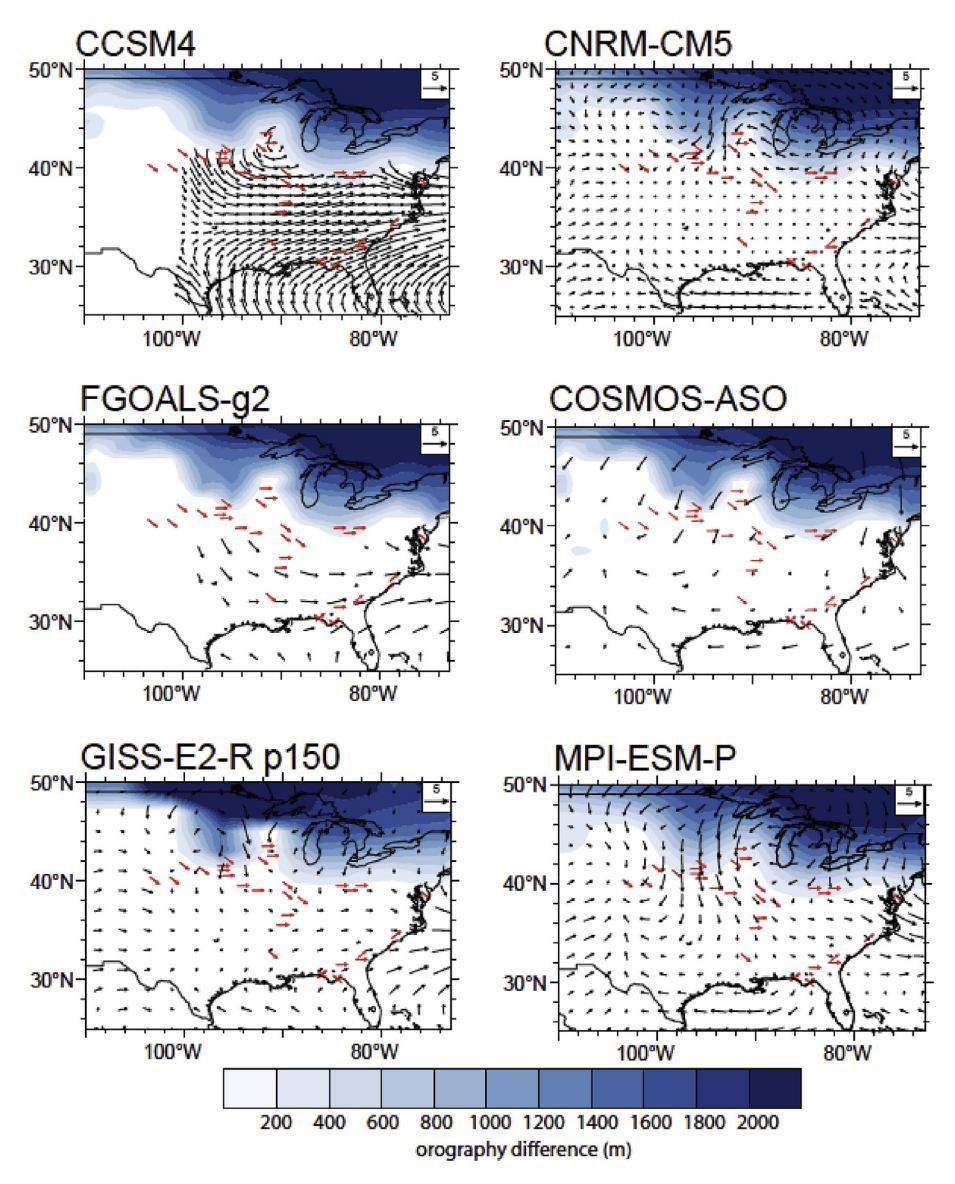


Fig. 3. Boreal spring (MAM) LGM surface wind vectors for the top (left column) and bottom (right column) three ranking PMIP3 models (Table 4). Ice sheet elevation shown in blue. Paleovectors are in red. FGOALS and CCSM4 do not archive near surface winds or winds at geopotential heights below the actual land surface, so 925 mb winds are plotted. Please refer to Supplemental Figs. 2 and 3 for 850 mb and 700 mb winds in CCSM4 and FGOALS, and Supplemental Fig. 5 for comparison of MAM pre-industrial control and LGM winds for all models.

similar to modern meridional wind direction, although the upper Midwest still receives northerly flow off the ice sheet in many models in the summer season. The latitude of the transition from northerly to southerly winds varies substantially from model to model. Across all seasons, the COSMOS model stands out as an outlier, with easterly winds across North America in fall, spring, and summer as well as in winter east of 94°W.

Proxy-model zonal and meridional wind direction agreement varies strongly from model to model and by season (Fig. 6). Overall there is most agreement with zonal wind direction in winter (mean  $\pm$  1 standard deviation AC1 score of  $0.81 \pm 0.16$ ). In spring and fall, many models also agree with the proxy data, indicating westerly winds, but the range of agreement across models is larger (mean spring AC1 score of  $0.54 \pm 0.50$ , and fall,  $0.44 \pm 55$ ). Summer model-data zonal wind direction agreement is weak (mean AC1 score of  $0.02 \pm 0.67$ ). Considering meridional wind data-model agreement in the 16 proxy locations with meridional wind information, the models show more agreement with the data

throughout the seasons, with spring showing the most models in agreement with the data (mean AC1 score of 0.67  $\pm$  0.23), followed by winter (mean AC1 score of 0.61  $\pm$  0.20), fall (mean AC1 score of 0.50  $\pm$  0.29), and summer (mean AC1 score of 0.45  $\pm$  0.36). We categorize the top 3 and bottom 3 performing models for each season based on the average of each model's zonal and meridional AC1 values (Table 4).

The high (p150) and low (p151) ice sheet simulations with GISS-E2-R offer an opportunity to examine the influence of ice sheet topography on surface winds. Both the high and low ice sheet simulations with GISS-E2-R appear in the list of top ranked models in different seasons (Table 2). GISS p150 is one of the bottom-ranked models in winter, although it is important to note that the model wind directions have strong overall agreement with the proxy-inferred wind direction in winter, and the GISS p150 score in winter is still quite high (0.62). Comparison of these two GISS LGM simulations with different ice sheet topography shows relatively minor changes in surface wind speed and direction over land in the

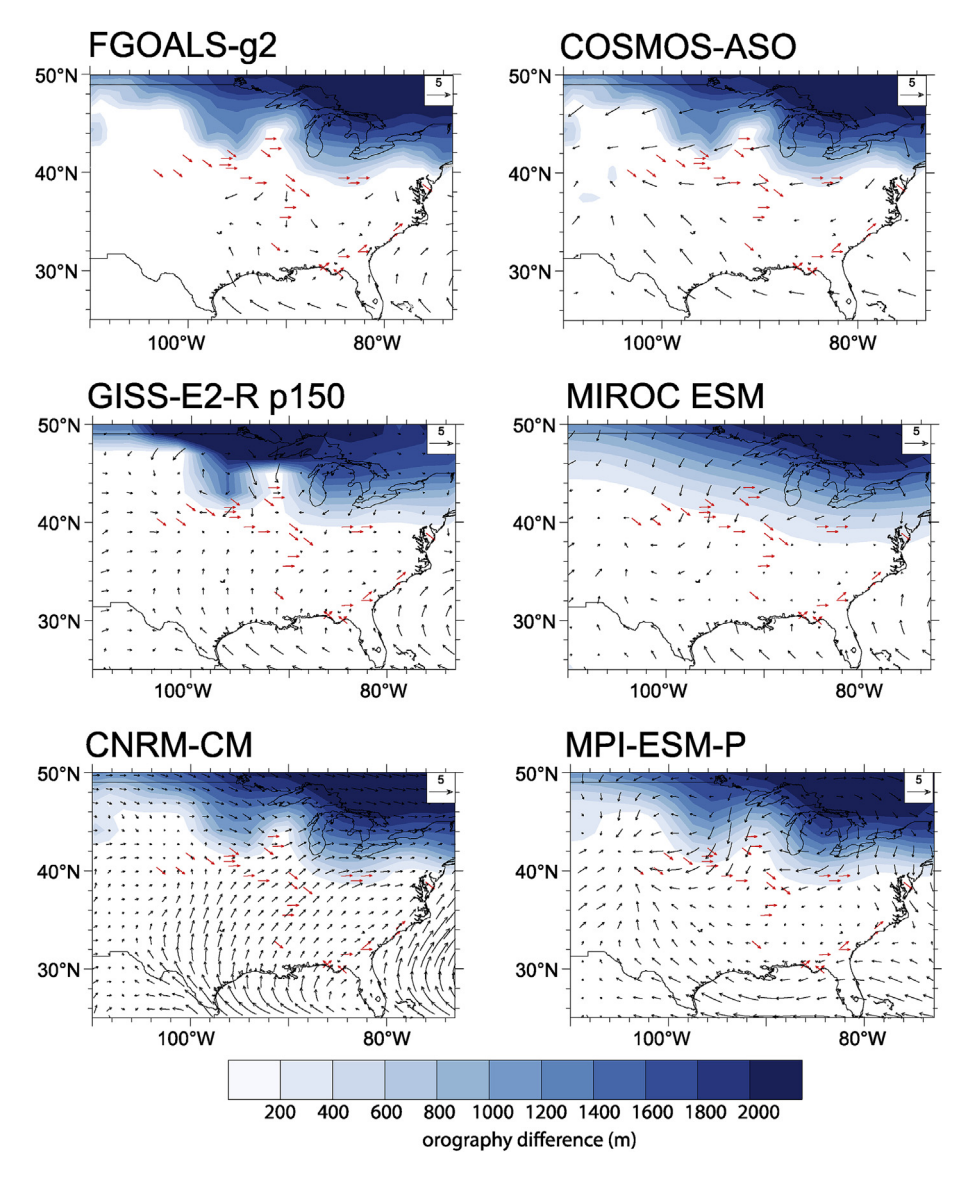


Fig. 4. Boreal summer (JJA) LGM surface wind vectors for the top (left column) and bottom (right column) three ranking PMIP3 models (Table 4). Ice sheet elevation shown in blue. Paleovectors are in red. FGOALS does not archive near surface winds or winds at geopotential heights below the actual land surface, so 925 mb winds are plotted. Please refer to Supplemental Fig. 3 for 850 mb and 700 mb winds in FGOALS, and Supplemental Fig. 6 for comparison of JJA pre-industrial control and LGM winds for all models.

study region (Supplemental Fig. 9). The largest changes in wind speed and direction occur where the ice margin and elevation differ. The p150 ice sheet is higher near the ice margin, and includes a feature similar to the Des Moines Lobe, leading to stronger winds in this area compared to p151. However, in both simulations, winds over the ice sheet are largely northerly to northeasterly.

All LGM simulations show prominent Aleutian and Icelandic Lows in SLP, accompanied by cyclonic circulation at the surface, and a Laurentide High over the ice sheet, accompanied by anticyclonic circulation at the surface (Figs. 7 and 8). The subtropical Bermuda High and North Pacific Highs are more prominently expressed in SLP in the subtropical North Atlantic Ocean and Pacific Oceans, respectively, in the summer season (Figs. 7 and 8). Across the nine models, there is variability in the magnitude and spatial extent of these large-scale areas of high and low SLP. The strength and spatial footprint of the Laurentide High is weaker and reduced in the models with the highest AC1 scores. In these same models, the Aleutian Low and Icelandic Low are also enhanced, whereas the Bermuda and North Pacific Highs are weaker (Figs. 7 and 8). In the

highest-ranking models, consistent with the weaker Laurentide High, the easterly winds at the Laurentide High's southern flank are constrained at the lower atmospheric levels and are tightly anchored to the ice sheet across all seasons (Fig. 9, left panel). The surface easterly winds do not extend south of 42°N-43°N and most proxy locations (Fig. 1) are within the surface westerly belt. On the contrary, in the lowest ranking models, the easterly winds are stronger and extend south of the ice sheet margin covering the proxy latitudes (Fig. 9, middle panel and left panel). Upper level winds (200 mb) are weaker over the ice sheet and just south of the ice sheet in the highest-versus the lowest-ranking models in all seasons, and the jet stream is shifted southward (Fig. 9). Accompanying simulated differences in SLP are differences in surface air temperature (Fig. 10). In models with a weaker Laurentide High, surface air temperature is warmer over the Laurentide Ice Sheet and over the North Atlantic Ocean.

The multimodel mean of the frequency of daily surface wind speeds greater than 8 m/s shows a greater number of days with winds above this threshold velocity during the LGM relative to the

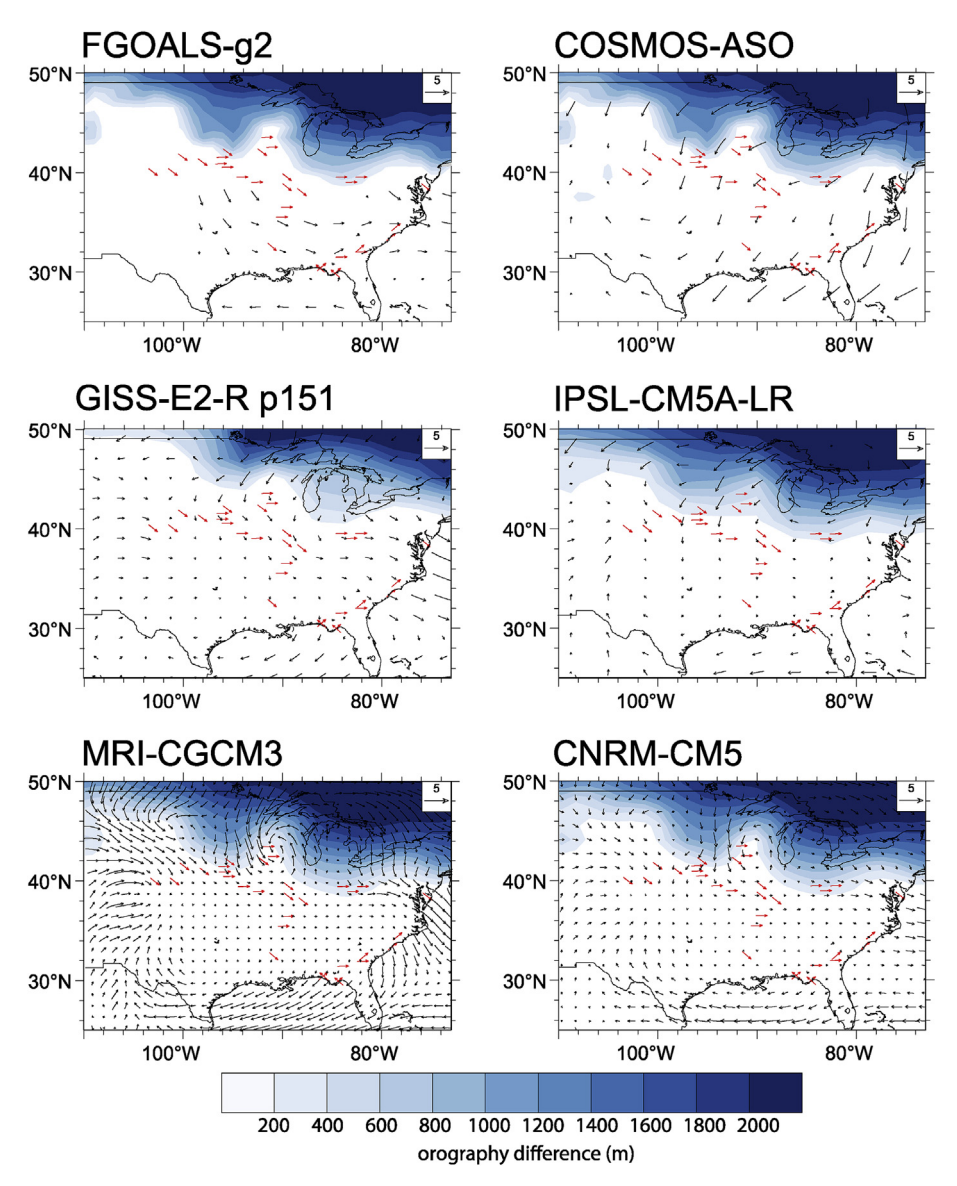


Fig. 5. Boreal fall (SON) LGM surface wind vectors for the top (left column) and bottom (right column) three ranking PMIP3 models (Table 4). Ice sheet elevation shown in blue. Paleovectors are in red. FGOALS does not archive near surface winds or winds at geopotential heights below the actual land surface, so 925 mb winds are plotted. Please refer to Supplemental Fig. 3 for 850 mb and 700 mb winds in FGOALS, and Supplemental Fig. 7 for comparison of SON pre-industrial control and LGM winds for all models.

pre-industrial control in winter, spring, and fall (Fig. 11). This also holds for the individual models, which generally show a greater number of fast wind days in the LGM if the pre-industrial control also has a higher number of fast wind days. There is not a relationship between seasonal averaged zonal and meridional AC1 scores (used to rank the models) and fast wind day frequency in the LGM (r=-0.11, p=0.64, N=20).

## 4. Discussion

The strong agreement between model and proxy LGM wind direction suggests the many of the latest generation of GCMs, when combined with the most recent ice sheet models, are accurately simulating LGM climate over midcontinental and eastern North America. Westerly near-surface zonal winds are predominant south of the ice sheet margin, in line with aeolian proxy data. The latitudinal transition from northerly to southerly meridional winds is also captured in many simulations. However, there is a range of model-data agreement values, especially in spring, fall, and

summer (Fig. 6), which permits further investigation into the differences in drivers of surface wind direction in models that agree well and models that agree poorly with the proxy data. In the following sections, we assess these possible controls (Section 4.1), followed by a deeper inquiry into the seasonality of LGM aeolian transport and deposition, which remains uncertain (Section 4.2). Finally, we consider the temporal frequency of loess entrainment and deposition by assessing the frequency of high wind speeds in daily-resolved model output in the context of the seasonality of aeolian deposition (Section 4.3).

## 4.1. Controls on LGM surface wind direction

Over the study area, surface wind direction is influenced by surface pressure and the strength and location of the prominent semi-permanent pressure systems in the North Pacific, North Atlantic, and over the Laurentide Ice Sheet (Figs. 7 and 8). We find distinct SLP patterns in the models with the highest and lowest AC1 scores with the proxy data. Comparing multimodel mean SLP for

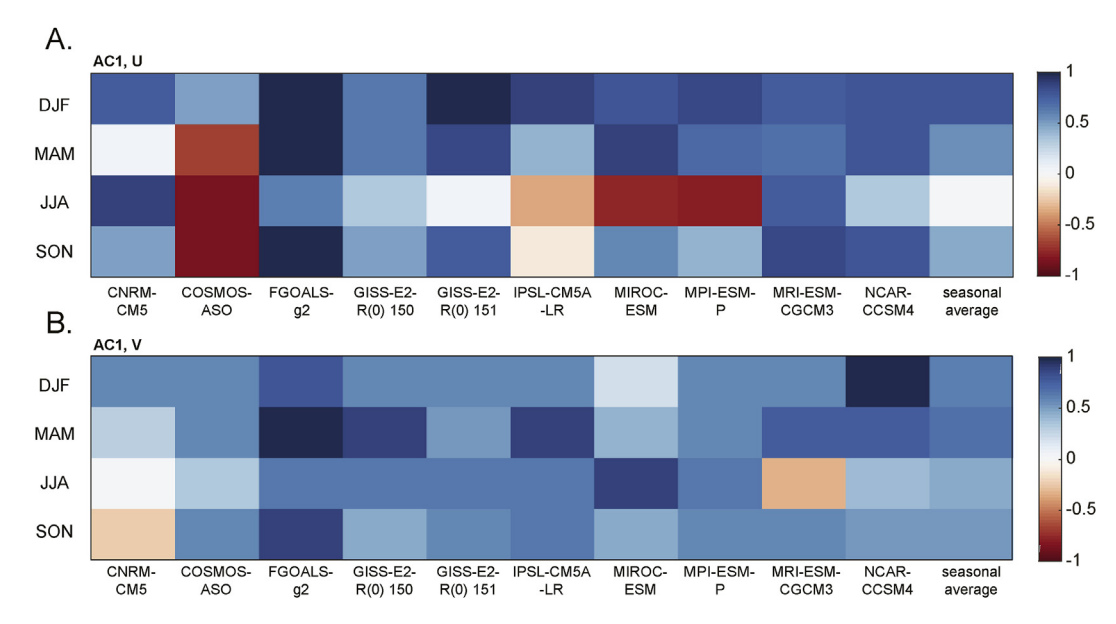


Fig. 6. Gwet's AC1 values by season, expressing the agreement between the A) the zonal component of the 30 paleowind vectors and the zonal component of the model wind vectors (Table 1) and B) the meridional component of the 16 paleowind vectors with meridional wind direction information (Table 1) and the meridional component of the model wind vectors. The average model AC1 value for each season is also plotted on the far right.

**Table 3**Distribution of model and proxy data by rater and response category, after Gwet (2002), Table 1.

Rater B (Model)	Rater A	Total	
	1 (westerly)	2 (easterly)	
1 (esterly)	A	В	B1 = A + B
2 (easterly)	C	D	B2 = C + D
Total	A1 = A + C	A2 = B + D	N

**Table 4**Top three and bottom three ranked models, based on the mean of the model zonal and meridional AC1 scores, for each season.

Season	Top 3 Models	Bottom 3 Models
Winter (DJF)	FGOALS	COSMOS
	CCSM4	MIROC
	GISS p151	GISS p150
Spring (MAM)	FGOALS	COSMOS
	CCSM4	CNRM
	GISS p150	MPI
Summer (JJA)	FGOALS	COSMOS
,	GISS p150	MPI
	CNRM	MIROC
Fall (SON)	FGOALS	COSMOS
	GISS p151	CNRM
	MRI	IPSL

the top three and bottom three ranked models (in terms of mean zonal and meridional AC1 scores), several strong differences emerge (Fig. 8). The models with the top AC1 scores in winter have a weaker Laurentide High more confined to the ice sheet, and an enhanced Aleutian Low and Icelandic Low. These low pressure areas also extend closer to the North American continent in the top three models. This likely constrains the spatial footprint of the Laurentide High, keeping it, and the northeasterly winds on its eastern side, to the north of the ice sheet margin. In models with the lowest agreement between model and proxy wind direction, the Laurentide High is stronger, and high pressure over the ice sheet extends well past the ice sheet margin. This ultimately leads

to more northeasterly winds, disagreeing with the westerly winds implied by the proxy data. In summer, spring, and fall, the top performing models also have a weaker Bermuda High. Although the Bermuda High does not seem to bring more easterly winds over our study region, a stronger and more westerly oriented Bermuda High may enhance southerly winds over the southern portion of our study area. In sum, the strength and position of major high and low semi-permanent pressure systems vary from model to model and are tightly linked to surface wind direction.

The location of the upper level jet stream is not the main control on near-surface zonal wind direction in the study region. Upper level (200 mb) zonal wind direction is consistently westerly across North America, including across the Laurentide Ice Sheet and south of the ice margin (Fig. 9, Supplemental Fig. 8). Near-surface zonal wind direction is more variable from model to model (Fig. 8, Supplemental Figs. 4–7). Thus, even with a southward shifted jet stream at upper levels of the atmosphere, the main influence on the zonal direction of near-surface winds, which are recorded by the loess and dune deposits, is how tightly the near-surface easterly winds are constrained to the ice sheet. In models with a weaker Laurentide High constrained to the ice sheet, the near-surface easterly winds also remain over the ice sheet, and do not extend past the ice sheet margin (Fig. 9).

Models that agree best with the proxy wind direction data and have a smaller and weaker Laurentide High also have warmer surface air temperatures above the ice sheet and in the North Atlantic and slightly cooler temperatures over large parts of unglaciated North America to the south of the ice sheet (Fig. 10). This pattern occurs in every season, leading to differences in the ocean-land temperature contrast between the two model groups, and consequent differences in stationary wave patterns. Stationary waves play a significant role in determining the zonal shifts and meandering of the jet streams, as well as the location of semi-permanent highs and lows (Brayshaw et al., 2009; Karamperidou et al., 2012; Merz et al., 2015), and may ultimately be the driver of the observed differences in SLP and surface wind direction.

A possible driver of the LGM differences in surface temperature and SLP is the topography of the Laurentide Ice Sheet. A relationship between ice sheet topography, stationary waves, and

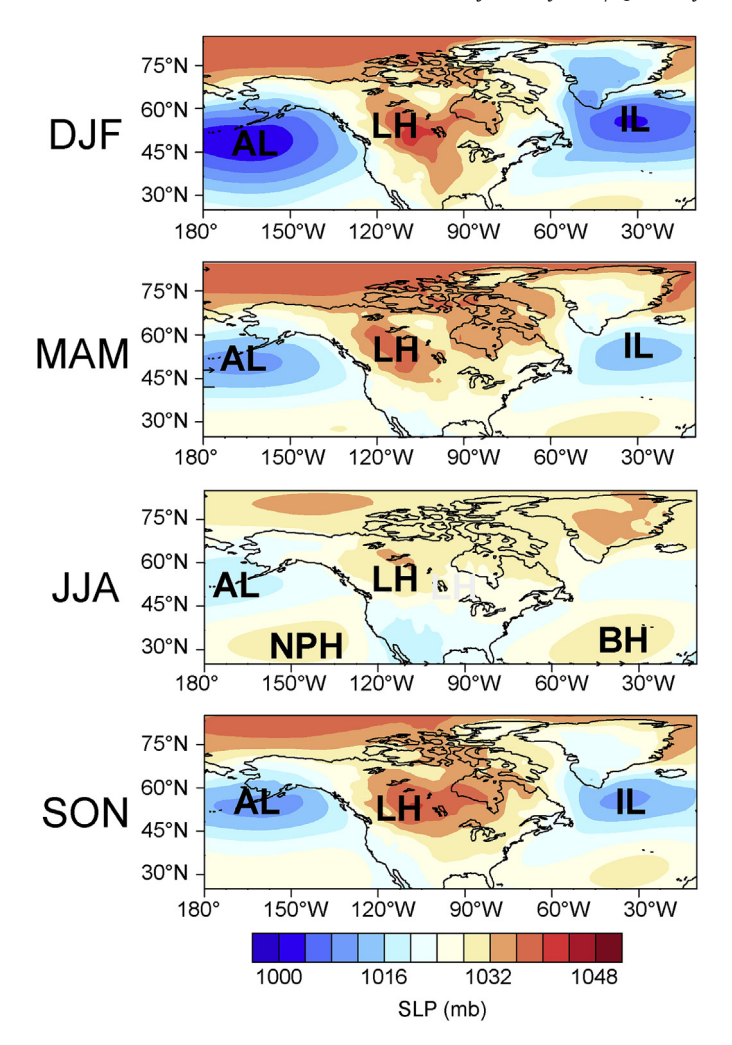


**Fig. 7.** The semi-permanent pressure systems discussed in the text. Seasonal multimodel mean SLP (colored contours) is plotted for the three models with the highest AC1 scores (Table 4). LH: Laurentide High, AL: Aleutian Low, IL: Icelandic Low, BH: Bermuda High, NPH: North Pacific High.

downstream climate has been observed using a linear model, an atmospheric GCM, and a coupled land-atmosphere GCM (Liakka et al., 2012; Löfverström et al., 2014). As pointed out in Pausata et al. (2009), differences in model physics and/or parameterizations are presumably responsible for the various degrees of sensitivity of the LGM wind response to ice sheet topography. Pausata et al. (2011) and Merz et al. (2015) also showed in experiments with two state-of-the-art fully coupled models (IPSL CM4-V1 and CCSM4, respectively) that the height of the Laurentide Ice Sheet plays an important role in determining the magnitude of the LGM shifts of both the 200 mb jet stream and the low-level (925-700 mb) eddy-driven jet, the latter of which is tied to the locations of semi-permanent high and low pressure systems. CCSM4 is one of the models participating in PMIP3, and shows good agreement with the paleo-wind proxies (Fig. 6), whereas IPSL CM4-V1 participated in PMIP2 and is not analyzed in the present study. However, our results with the GISS simulations with different ice sheet topographies suggest large differences in ice sheet topography cannot be implicated as the cause of the different temperature and pressure patterns in models with strong and weak agreement with the proxy wind direction data. In the case of the two GISS simulations, both the high and low elevation ice sheets produce surface winds that agree with the proxy data in different seasons (Table 4). Furthermore, there are not substantial differences in the ice sheet topographies of the other top or bottomranking models (Supplemental Fig. 1), although LGM topography for FGOALS and COSMOS were not archived.

Model biases may also explain the inter-model differences. Such biases can persist between very different climate states, with largescale, global patterns of many climate variables highly correlated between an individual model's pre-industrial and 4 times CO<sub>2</sub> simulation (Krinner and Flanner, 2018). To investigate whether persistent model biases can explain the inter-model differences observed in the LGM, we compared the differences between surface air temperature, SLP, and 925-700 mb winds for the multimodel means of the three top and bottom-ranked models in both the LGM and pre-industrial control simulations (Supplemental Fig. 10). If model biases are the primary cause of the observed inter-model differences, and are stationary between different climate states, we would observe similar patterns of these three variables in the LGM and pre-industrial figures. We find that temperature difference patterns are not similar between the two climate states; overall, the top-ranking models have colder land and warmer oceans compared to the bottom-ranking models. The regions of model disagreement in temperature loosely correspond to regions where inter-model differences can be linked to the simulated net cloud feedback (Soden and Vecchi, 2011; Zelinka et al., 2016; Ceppi et al., 2017). That is, the change in radiative flux at the top of the atmosphere due to changes in properties of clouds that influence both the reflection of incoming shortwave radiation and the absorption of outgoing longwave radiation. The simulation of clouds in climate models and their role in determining climate sensitivity is one of the leading uncertainties in future climate projections (Bony and Dufresne, 2005); further attention to this issue in paleoclimate studies may help reduce these uncertainties. With respect to SLP, the Aleutian Low and associated winds appear to be stronger in both the LGM and pre-industrial simulations in the top models. Winds between the 925 and 700 mb level across eastern North America and the Atlantic Ocean, which comprise the eddy-driven jet stream, are also weaker in winter in both the LGM and preindustrial simulations, and lower SLP anomalies and anomalous cyclonic flow are also observed in the Atlantic in spring, summer and fall in both simulations. Thus, some, but not all aspects of largescale circulation in the study region may be influenced by persistent model biases possibly associated with model simulation of the main climate feedbacks. A full consideration of the stationarity of large-scale climate biases between past extreme climate states and an assessment of the balance of climate feedbacks in these models is beyond the scope of this study, but these preliminary conclusions suggest some stationarity in potential biases in these climate variables during the LGM and pre-industrial control climates of this region.

#### 4.2. Seasonality of LGM aeolian activity

The most recent generation of GCMs participating in the PMIP3 LGM climate experiment show an overall large degree of agreement with inferred proxy wind direction over midcontinental and eastern North America. However, the question of the seasonality of LGM dustiness and related aeolian deposition has not yet been sufficiently resolved, and partly motivated the present assessment of model-proxy agreement in all four seasons. Previous proxymodel comparisons of LGM wind direction have focused on winter, sometimes contrasted with summer, but spring and fall may have also been seasons of loess deposition and aeolian activity. It is likely that winter has typically been the focus of previous datamodel comparisons given it is the season of strong winds and frontal storms, accompanied by a lack of sediment-anchoring

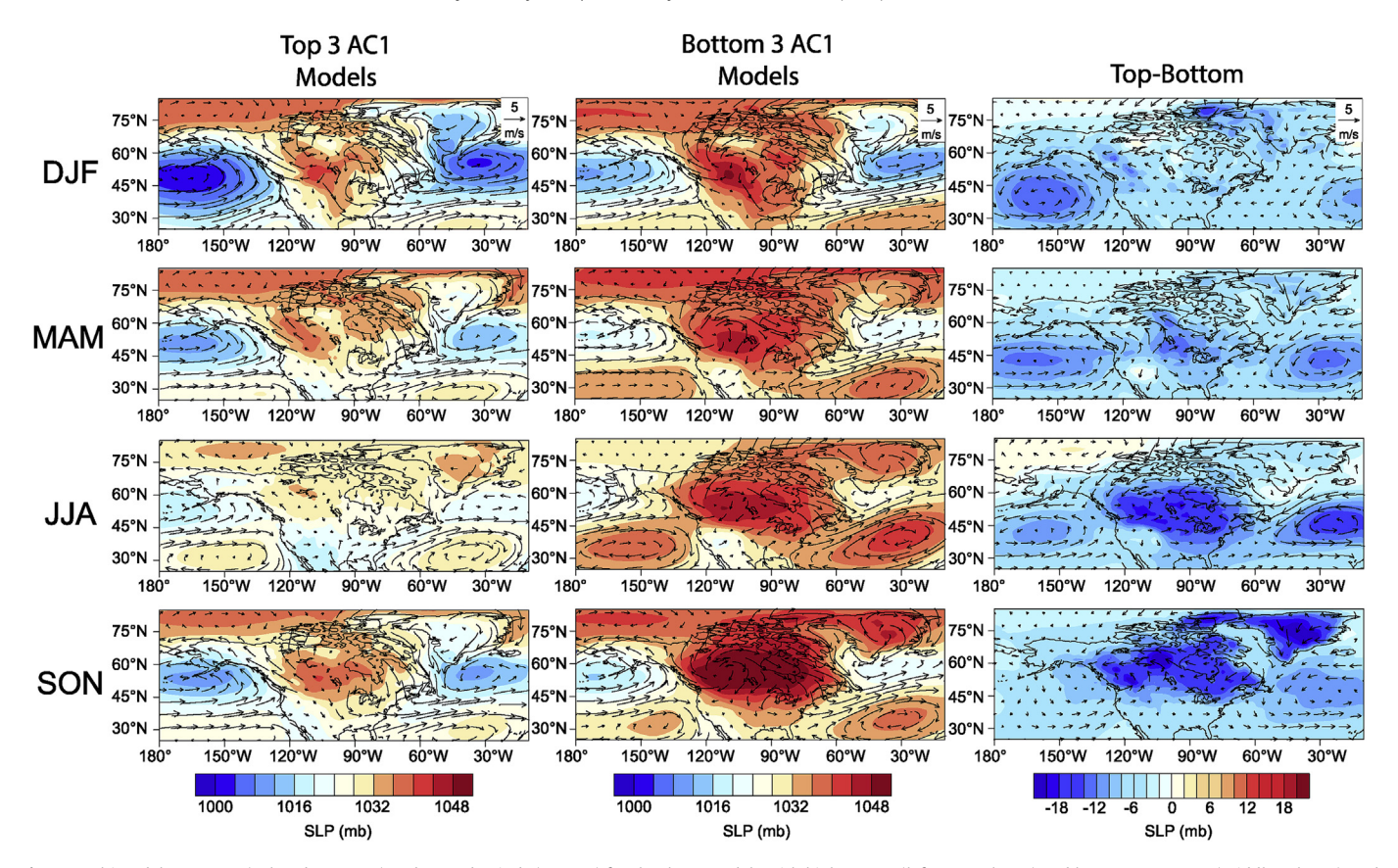


Fig. 8. Multimodel mean SLP (colored contours) and 925 mb winds (vectors) for the three models with highest AC1 (leftmost column) and lowest AC1 scores (middle column), and the difference in the multimodel means (rightmost column), for each season (rows). Vector scale (5 m/s) for each set of maps given in top row of maps.

vegetation on the landscape, especially near the ice margin during the LGM. However, snow cover as well as permafrost may limit aeolian deflation during the winter season, as noted by modern dust observations at high latitudes (Crusius et al., 2011; Bullard et al., 2016; Bullard and Mockford, 2018). Summer is less frequently considered the season of loess deposition, although summer loess deposition and dustiness occur in some high-latitude proglacial environments, as it is the season of peak melting, runoff, and sediment supply (Fehrenbacher et al., 1965; Bullard et al., 2016). However, hydrologic conditions in meltwater valleys during the summer melt season are less conducive to drying of silts and dust entrainment. Observations also support fall aeolian activity and dustiness in high northern latitudes today. For example, along the Copper River Valley in Alaska, remote sensing shows dust events mainly occur during the fall, following the summer meltwater season. In this season, rivers levels decrease, valley sediments dry, and there is limited snow cover. This set of conditions permits fine, unconsolidated, glaciofluvial sediment to be exposed to the atmosphere and entrained locally to regionally as dust (Crusius et al., 2011). Similarly, as glacial river valleys dried out in the LGM fall, exposing unconsolidated, fine-grained glaciofluvial sediment to the atmosphere, this may have been a key season for silt entrainment and loess deposition (Leighton and Willman, 1950). Spring, the season of strong cyclogenesis and cold fronts in the mid-latitudes, has also been considered an important season for dust transport in northern China (Roe, 2009). Modern dust studies adjacent to the Greenland ice sheet margin find peak dustiness in both the spring and fall due to the timing of strong winds, soil hydrological conditions, snow cover, and sediment supply (Bullard and Mockford, 2018).

Our results suggest winter is the month with the best overall

agreement between model and proxy wind direction, but in some models, strong agreement also occurs during the spring and fall. Consideration of important factors beyond wind speed, such as snow cover, permafrost, valley hydrology, soil moisture, and vegetation cover in modern high latitude environments influenced by glaciers helps support spring and fall as likely seasons of aeolian sedimentation (Bullard et al., 2016). Thus, we conclude, at least for the midcontinent locations, that loess deposition and aeolian activity was most probable, and more frequent, in these seasons. Along the Atlantic Coastal Plain, dune migration could also have occurred in multiple seasons. As presented in the results section, more models capture the correct southerly wind direction on the southern Atlantic Coastal Plain in both spring and winter.

### 4.3. LGM surface wind speeds and aeolian activity

Modern dust studies show the necessity of cold-air outbreaks and associated frontal storms for entraining and transporting dust (e.g., Roe, 2009). These outbreaks, which occur on the synoptic scale and propagate from west to east across midcontinental North America, offered a resolution to previous mismatches between mean easterly winds in coarse, monthly resolved climate model simulations and westerly winds archived in aeolian deposits (Muhs and Bettis, 2000). As many models now show westerly mean, climatological winds, there is less of a need to invoke disparate temporal scales of wind direction, but modern process-based studies still speak to the importance of short-term weather events in entraining and transporting dust (Roe, 2009; McGee et al., 2010; Crusius et al., 2011; Sweeney and Mason, 2013). Most PMIP3 LGM output remains monthly in resolution, hindering investigation of the role of short-term periods of enhanced westerly winds. One

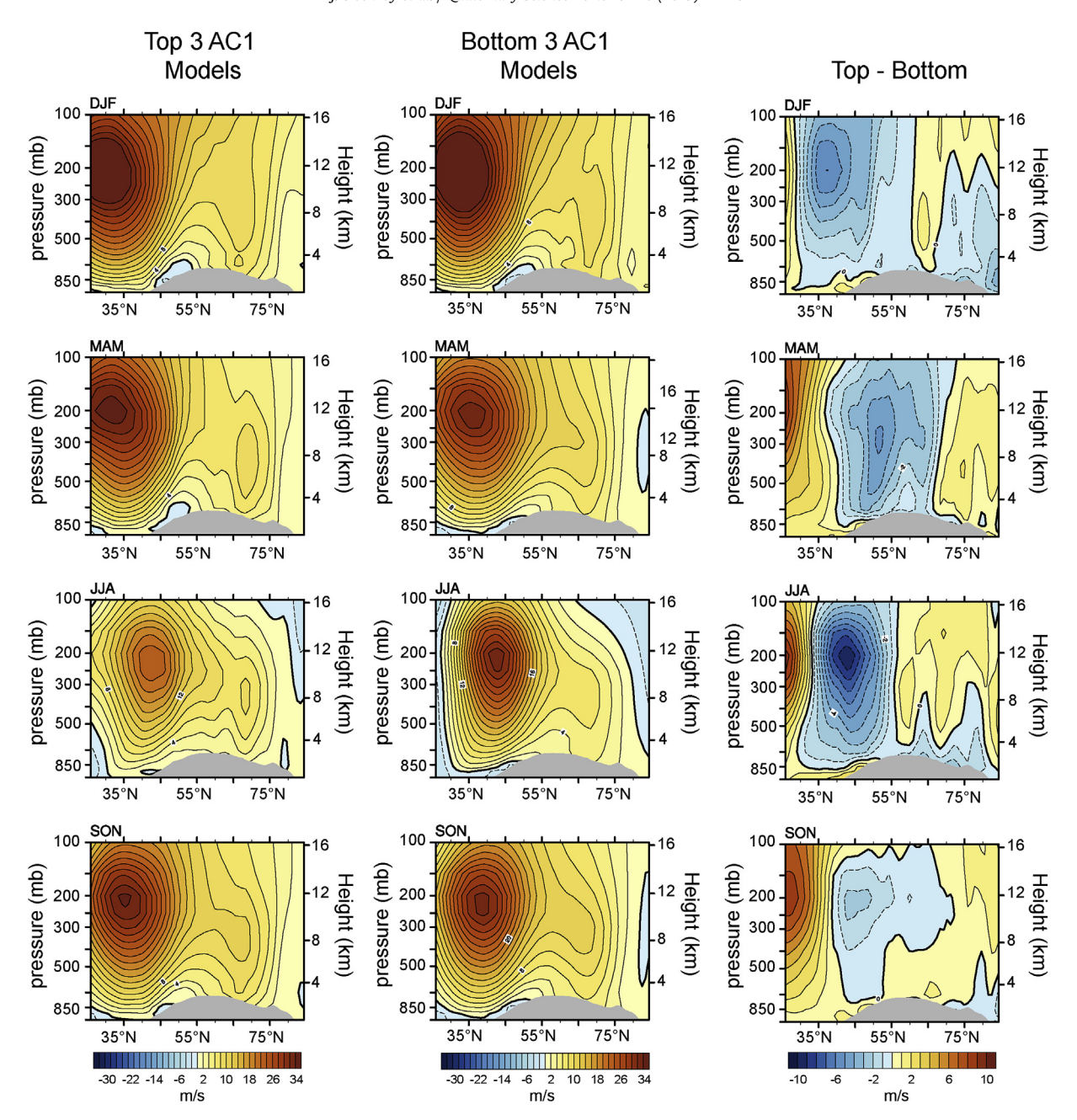


**Fig. 9.** Vertical cross-sections of multimodel mean zonal wind speed (m/s) in the LGM averaged over 90°W-100°W (see Fig. 1) for the three models with highest AC1 (leftmost column) and lowest AC1 scores (middle column), and the difference in the multimodel means (rightmost column), for each season (rows). Positive values indicate westerly winds. The gray shaded area shows the difference in orography between LGM and piControl, indicating the extent of the ice sheet. Note that to create the ensemble means among models with different grids, the winds were extrapolated to the 1000 mb level and vertically regridded using linear interpolation. The ice sheet extent is plotted after height was converted to pressure level based on the 1976 U.S. standard atmosphere and masks extrapolated wind speed values.

CMIP5 variable, 'daily maximum near surface wind speed' (*SfcwindMax*) is ideal to address this issue, but it is not archived for LGM simulations. Thus, we explore the frequency of high daily wind speeds at the LGM using daily mean near-surface wind speed, which has been archived for the LGM and pre-industrial control simulations of CCSM4, COSMOS-ASO, MIROC, MRI, and MPI (Fig. 11). We chose 8 m/s as the threshold speed to entrain silt-sized particles (Sweeney et al., 2008; McGee et al., 2010; Sweeney and Mason, 2013). We also investigated the frequency of winds greater than or equal to 16 m/s, which was used as the threshold to define 'gusty' conditions in McGee et al. (2010). However, we did not find any mean daily wind speeds that surpassed this value,

given that we are limited to daily averages.

The LGM is hypothesized to be a period of greater gustiness, given the strong meridional temperature gradients at this time (McGee et al., 2010). In PMIP3 LGM simulations over midcontinental North America, climatological mean monthly near-surface winds are not consistently stronger at all grid points during the LGM versus the pre-industrial control, but vary in their magnitude spatially (Figs. 2–5). This was also noted by Mason et al. (2011) who showed weaker LGM winds in some locations in North America in earlier LGM simulations. However, the daily wind frequency analysis (Fig. 11A) does support the LGM as a period of faster wind speeds over the broader study region. Across all models, the

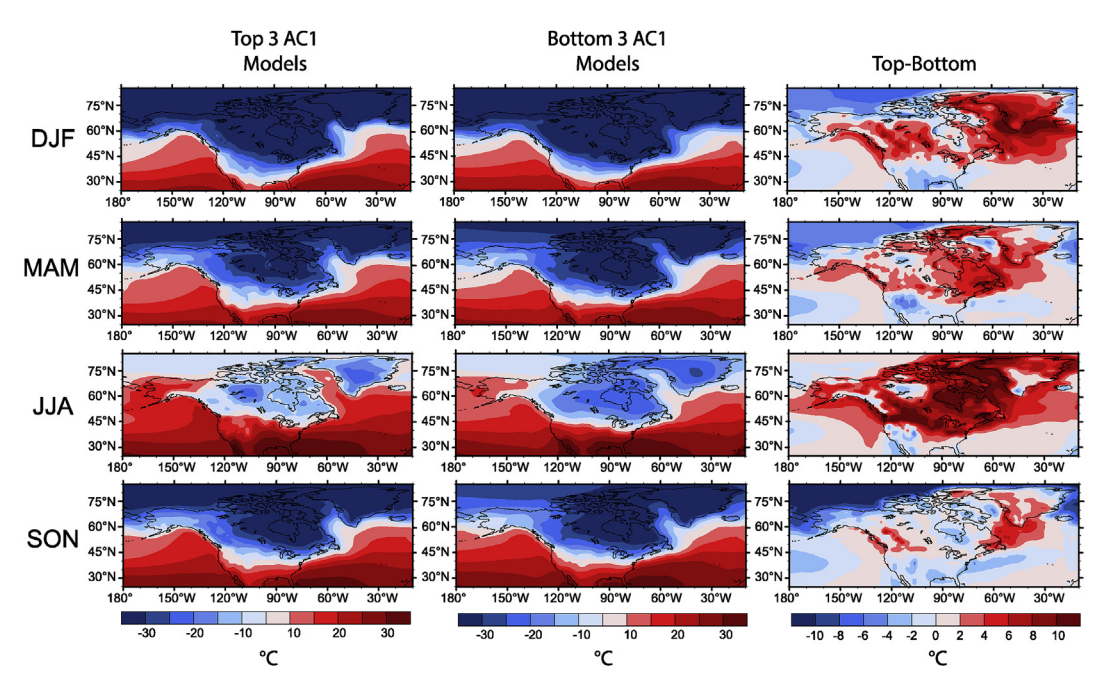
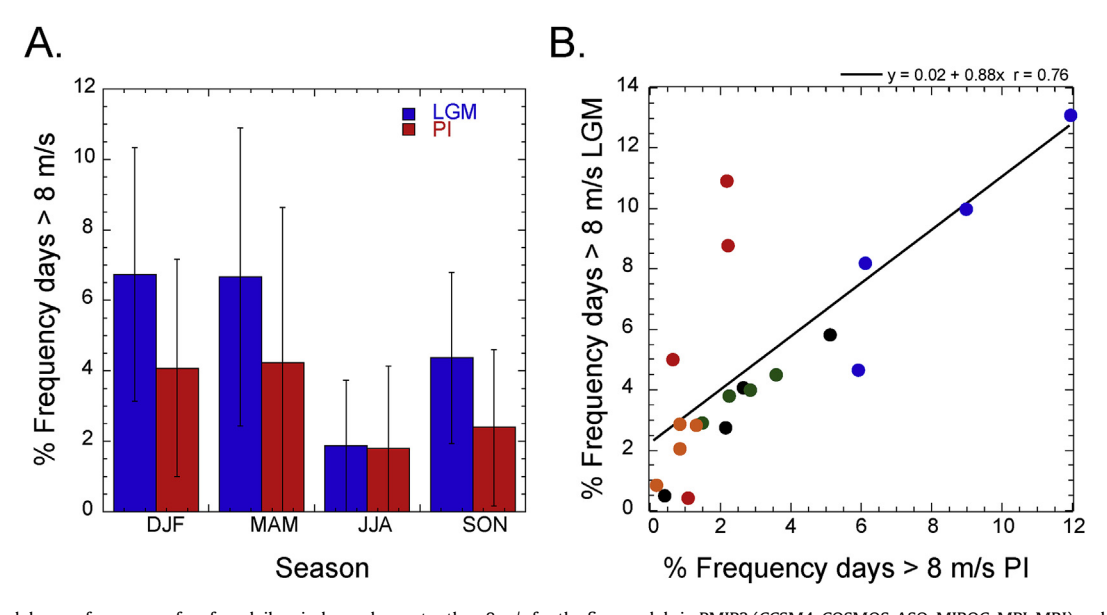


Fig. 10. Multimodel mean surface air temperature (colored contours) for the three models with highest AC1 (leftmost column) and lowest AC1 scores (middle column), and the difference in the multimodel means (rightmost column), for each season (rows).



**Fig. 11.** A) Multimodel mean frequency of surface daily wind speeds greater than 8 m/s for the five models in PMIP3 (CCSM4, COSMOS-ASO, MIROC, MPI, MRI) archiving this variable for the LGM (blue) and pre-industrial (red) simulations. Black line indicates one standard deviation. B) Scatterplot of monthly mean frequency of surface daily wind speeds greater than 8 m/s for each season of the five models in the LGM versus the pre-industrial simulations. Black: CCSM4, blue: COSOMOS, red: MIROC, green: MPI, orange: MRI.

LGM has a greater number of days with winds greater than 8 m/s, relative to the pre-industrial control. There is substantial intermodel variability in fast wind speed frequency, but winter and spring have the greatest number of fast wind days in the LGM, followed by fall. Summer has the lowest number of fast wind days and this number is similar in the LGM and pre-industrial control simulations. Thus, in the context of the seasonality of loess deposition, these data, like surface wind direction, point to winter, spring, and fall as viable seasons of silt entrainment and loess deposition, as well as overall aeolian activity. However, this analysis of fast-wind frequency also shows that models with more frequent fast winds in the pre-industrial control simulation also have more

frequent fast winds in the LGM, pointing again to the importance of considering model biases in assessment of gustiness in past climate states (Fig. 11B).

## 5. Conclusions

A persistent model-proxy data mismatch regarding the direction of near-surface winds during the LGM has challenged our understanding of terrestrial surface wind variability over the last several decades. Here we have demonstrated a high level of model-proxy data agreement for near surface wind direction in LGM simulations using output from the generation of comprehensive

earth system models participating in PMIP3. However, there is still variability in agreement from model to model and across seasons, permitting a deeper inquiry into the drivers of near-surface wind direction and its seasonal variability. Winter is the season of the highest agreement between model and proxy wind direction, followed by spring and fall. The models with the strongest agreement with proxy-inferred wind direction have a distinct SLP pattern. with a weaker Laurentide High, a stronger and more eastward Aleutian Low, and a stronger and more westward Icelandic Low. In these models northeasterly winds associated with the Laurentide High are more constrained spatially to the Laurentide Ice Sheet. This SLP pattern is accompanied by warmer surface air temperatures over the Laurentide Ice Sheet and the North Atlantic and cooler temperatures over North America south of the ice margin. Surface wind direction in models that agree poorly with the proxy data have a stronger and more spatially expansive Laurentide High, with high pressure extending south past the ice margin, bringing northeasterly winds into midcontinental North America.

Dust events, loess deposition, and aeolian activity occur at higher frequency time scales than the monthly resolution of climate model output, so we also investigated the frequency of days with strong winds, by season, in five models that archived daily surface wind speed. We find more days with faster mean wind speeds, greater than 8 m/s, in the LGM winter, spring, and fall relative to pre-industrial control. Days with fast winds occur most frequency in winter and spring, followed by fall, in agreement with the seasons of highest agreement between model and data wind direction. Thus, this model-proxy synthesis supports winter, spring, and fall as likely seasons of aeolian activity at the LGM.

This synthesis also highlights the improved ability of GCMs to simulate LGM terrestrial wind direction and the sensitivity of surface wind regimes to boundary conditions and model biases. Similar to recent conclusions regarding the drivers of large-scale hydroclimate during the LGM (Oster et al., 2015), the conclusions from this study emphasize the need to consider the strength and location of major semi-permanent high and low pressure systems in driving near-surface climate. Finally, as aeolian processes occur at shorter timescales, there is a continued need for high-resolution, weather-resolving paleoclimate simulations to understand processes represented in aeolian paleoclimate archives.

#### 6. Author statement

JLC, DAG, and WRG conceptualized the project, JLC, DAG, and WRG acquired funding. JLC designed the investigation and developed the methodology, JLC and CK conducted the analyses, and JLC wrote the paper. All authors helped edit the paper.

## Acknowledgements

This work was funded by the United States National Science Foundation (NSF-GLD 1637481) to JLC, DAG, and WRG and NSF-AGS 1602580 to JLC. CK is supported by NSF-AGS 1602097. This is UH SOEST contribution 10747. We thank B.B. Curry and the anonymous reviewers for helpful comments that improved the paper.

## Appendix A. Supplementary data

Supplementary data to this article can be found online at https://doi.org/10.1016/j.quascirev.2019.07.003.

#### References

Aleinikoff, J.N., Muhs, D.R., Saner, R.R., Fanning, C.M., 1999. Late Quaternary loess in northeastern Colorado: Part II - Pb isotopic evidence for the variability of loess

- sources. Geol. Soc. Am. Bull. 111, 1876-1883.
- Aleinikoff, J.N., Muhs, D.R., Bettis, E.A., Johnson, W.C., Fanning, C.M., Benton, R., 2008. Isotopic evidence for the diversity of late Quaternary loess in Nebraska: glaciogenic and nonglaciogenic sources. Geol. Soc. Am. Bull. 120, 1362–1377.
- Barnes, E.A., Polvani, L., 2013. Response of the midlatitude jets, and of their variability, to increased greenhouse gases in the CMIP5 models. J. Clim. 26, 7117–7135.
- Bettis, E.A., Muhs, D.R., Roberts, H.M., Wintle, A.G., 2003. Last glacial loess in the conterminous USA. Quat. Sci. Rev. 22, 1907—1946.
- Bony, S., Dufresne, J.L., 2005. Marine boundary layer clouds at the heart of tropical cloud feedback uncertainties in climate models. Geophys. Res. Lett. 32 https://doi.org/10.1029/2005GL023851.120806.
- Braconnot, P., Harrison, S.P., Kageyama, M., Bartlein, P.J., Masson-Delmotte, V., Abe-Ouchi, A., Otto-Bliesner, B., Zhao, Y., 2012. Evaluation of climate models using palaeoclimatic data. Nat. Clim. Change 2. 417.
- Brayshaw, D.J., Hoskins, B., Blackburn, M., 2009. The basic ingredients of the north Atlantic storm track. Part I: land—sea contrast and orography. J. Atmos. Sci. 66, 2539–2558.
- Bromwich, D.H., Toracinta, E.R., Oglesby, R.J., Fastook, J.L., Hughes, T.J., 2005. LGM summer climate on the southern margin of the Laurentide Ice Sheet: wet or dry? I. Clim. 18. 3317–3338.
- Bromwich, D.H., Toracinta, E.R., Wei, H., Oglesby, R.J., Fastook, J.L., Hughes, T., 2004. Polar MM5 simulations of the winter climate of the Laurentide ice sheet at the LGM. J. Clim. 17, 3415–3433.
- Bullard, J.E., Baddock, M., Bradwell, T., Crusius, J., Darlington, E., Gaiero, D., Gasso, S., Gisladottir, G., Hodgkins, R., McCulloch, R., McKenna-Neuman, C., Mockford, T., Stewart, H., Thorsteinsson, T., 2016. High-latitude dust in the Earth system. Rev. Geophys. 54. 447–485.
- Bullard, J.E., Mockford, T., 2018. Seasonal and decadal variability of dust observations in the Kangerlussuaq area, west Greenland. Arctic Antarct. Alpine Res. 50. S100011.
- Carver, R.E., Brook, G.A., 1989. Late Pleistocene paleowind directions, Atlantic coastal-plain, United-states. Palaeogeogr. Palaeocl. 74, 205–216.
- Ceppi, P., Brient, F., Zelinka, M.D., Hartmann, D.L., 2017. Cloud feedback mechanisms and their representation in global climate models. Wiley Interdiscip. Rev.: Clim. Change 8, e465.
- COHMAP, 1988. Climatic changes of the last 18,000 Years: observations and model simulations. Science 241, 1043–1052.
- Crusius, J., Schroth, A.W., Gasso, S., Moy, C.M., Levy, R.C., Gatica, M., 2011. Glacial flour dust storms in the Gulf of Alaska: hydrologic and meteorological controls and their importance as a source of bioavailable iron. Geophys. Res. Lett. 38. L06602, doi:06610.01029/02010GL046573.
- Ebens, R.J., Connor, J.J., 1980. Geochemistry of Loess and Carbonate Residuum. U.S. Geological Survey Professional Paper 954-G.
- Fehrenbacher, J.B., White, J.L., Ulrich, H.P., Odell, R.T., 1965. Loess distribution in southeastern Illinois and southwestern Indiana. Soil Sci. Soc. Am. Proc. 29, 566–572.
- Forman, S.L., Pierson, J., 2002. Late Pleistocene luminescence chronology of loess deposition in the Missouri and Mississippi river valleys, United States. Palaeogeogr. Palaeocl. 186, 25–46.
- Flato, G., Marotske, J., Abiodun, B., Braconnot, P., Chou, S.C., Collins, W., Cox, P.,
  Driouech, F., Emori, S., Eyring, V., Forest, C., Gleckler, P., Guilyardi, E., Jakob, C.,
  Kattsov, V., Reason, C., Rummukainen, M., 2013. Evaluation of climate models.
  In: Intergovernmental Panel on Climate, C. (Ed.), Climate Change 2013 the
  Physical Science Basis: Working Group I Contribution to the Fifth Assessment
  Report of the Intergovernmental Panel on Climate Change. Cambridge University Press, Cambridge, pp. 741–866.
- Frazee, C.J., Fehrenbacher, J.B., Krumbein, W.C., 1970. Loess distribution from a source. Soil Sci. Soc. Am. Proc. 34, 296–301.
- Frye, J.C., Glass, H.D., Willman, H.B., 1968. Mineral zonation of woodfordian loesses of Illinois. Ill. State Geol. Surv. Circ. 427, 44.
- Gan, B., Wu, L., Jia, F., Li, S., Cai, W., Nakamura, H., Alexander, M.A., Miller, A.J., 2017.

  On the response of the aleutian low to greenhouse warming. J. Clim. 30, 3007–3025
- Gwet, K., 2002. Kappa statistic is not satisfactory for assessing the extent of agreement between raters. Stat. Meth. Inter-Rater Reliab. Assess. 1, 1–5.
- Hallberg, G.R., 1979. Wind-aligned drainage in loess in Iowa. Proc. Iowa Acad. Sci. 86. 4–9.
- Handy, R.L., 1976. Loess distribution by variable winds. GSA Bull. 87, 915-927.
- Harrison, S.P., Bartlein, P.J., Prentice, İ.C., 2016. What have we learnt from palae-oclimate simulations? J. Quat. Sci. 31, 363–385.
- Ivester, A.H., Leigh, D.S., Godfrey-Smith, D.I., 2001. Chronology of inland eolian dunes on the Coastal Plain of Georgia, USA. Quat. Res. 55, 293–302.
- Ivester, A.H., Leigh, D.S., 2003. Riverine dunes on the Coastal Plain of Georgia, USA. Geomorphology 51, 289–311.
- Karamperidou, C., Cioffi, F., Lall, U., 2012. Surface temperature gradients as diagnostic indicators of midlatitude circulation dynamics. J. Clim. 25, 4154–4171.
- Kohfeld, K.E., Muhs, D.R., 2001. Midcontinental USA Gridded Maps of Loess Thickness. IGBP PAGES/World Data Center for Paleoclimatology, NOAA/NGDC Paleoclimatology Program, Boulder CO, USA.
- Krinner, G., Flanner, M.G., 2018. Striking stationarity of large-scale climate model bias patterns under strong climate change. Proc. Natl. Acad. Sci. Unit. States Am. 115, 9462–9466.
- Kulkarni, S., Huang, H.-P., 2014. Changes in surface wind speed over North America from CMIP5 model projections and implications for wind energy. Adv.

- Meteorol. 2014, 10.
- Kumar, D., Mishra, V., Ganguly, A.R., 2015. Evaluating wind extremes in CMIP5 climate models. Clim. Dyn. 45, 441–453.
- Kutzbach, J.E., Guetter, P.J., 1986. The influence of changing orbital parameters and surface boundary conditions on climate simulations for the past 18 000 years. J. Atmos. Sci. 43, 1726–1759.
- Leigh, D.S., Knox, J.C., 1994. Loess of the upper Mississippi valley driftless area. Quat. Res. 42, 30–40.
- Leighton, M.M., Willman, H.B., 1950. Loess formations of the Mississippi valley. I. Geol. 58, 599–623.
- Liakka, J., Nilsson, J., Löfverström, M., 2012. Interactions between stationary waves and ice sheets: linear versus nonlinear atmospheric response. Clim. Dyn. 38, 1249–1262.
- Licciardi, J.M., Clark, P.U., Jenson, J.W., Macayeal, D.R., 1998. Deglaciation of a softbedded Laurentide ice sheet. Ouat. Sci. Rev. 17, 427–448.
- Löfverström, M., Caballero, R., Nilsson, J., Kleman, J., 2014. Evolution of the large-scale atmospheric circulation in response to changing ice sheets over the last glacial cycle. Clim. Past 10, 1453–1471.
- Lora, J.M., 2018. Components and mechanisms of hydrologic cycle changes over North America at the last glacial maximum. J. Clim. 31, 7035–7051.
- Markewich, H.W., Litwin, R.J., Wysocki, D.A., Pavich, M.J., 2015. Synthesis on Quaternary aeolian research in the unglaciated eastern United States. Aeolian Research 17, 139—191.
- Mason, J.A., Nater, E.A., Hobbs, H.C., 1994. Transport direction of Wisconsinan loess in southeastern Minnesota. Quat. Res. 41, 44–51.
- Mason, J.A., 2001. Transport direction of Peoria loess in Nebraska and implications for loess sources on the central Great Plains. Quat. Res. 56, 79–86.
- Mason, J.A., Swinehart, J.B., Hanson, P.R., Loope, D.B., Goble, R.J., Miao, X., Schmeisser, R.L., 2011. Late pleistocene dune activity in the central Great Plains, USA. Quat. Sci. Rev. 30, 3858–3870.
- Matalucci, R.V., Shelton, J.W., Abdelhad, M., 1969. Grain orientation in vicksburg loess. I. Sediment. Petrol. 39, 969–979.
- loess, J. Sediment. Petrol. 39, 969–979.

  McGee, D., Broecker, W.S., Winckler, G., 2010. Gustiness: the driver of glacial dustiness? Quat. Sci. Rev. 29, 2340–2350.
- Merz, N., Raible, C.C., Woollings, T., 2015. North Atlantic eddy-driven jet in interglacial and glacial winter climates. J. Clim. 28, 3977–3997.
- Muhs, D.R., Aleinikoff, J.N., Stafford Jr., T.W., Kihl, R., Been, J., Mahan, S.A., Cowherd, S.D., 1999. Late Quaternary loess in northeastern Colorado, I: age and paleoclimatic significance. Geol. Soc. Am. Bull. 111, 1861–1875.
- Muhs, D.R., Bettis, E.A., 2000. Geochemical variations in Peoria Loess of western Iowa indicate paleowinds of midcontinental North America during last glaciation. Quat. Res. 53, 49–61.
- Muhs, D.R., Bettis, E.A., Been, J., McGeehin, J.P., 2001. Impact of climate and parent material on chemical weathering in loess-derived soils of the Mississippi river valley. Soil Sci. Soc. Am. J. 65, 1761–1777.
- Muhs, D.R., 2013. The geologic records of dust in the Quaternary. Aeolian Research 9, 3–48.
- Muhs, D.R., Bettis, E.A., Roberts, H.M., Harlan, S.S., Paces, J.B., Reynolds, R.L., 2013. Chronology and provenance of last-glacial (Peoria) loess in western Iowa and paleoclimatic implications. Quat. Res. 80, 468–481.
- Nash, T.A., Conroy, J.L., Grimley, D.A., Guenthner, W.R., Curry, B.B., 2018. Episodic deposition of Illinois Valley Peoria silt in association with Lake Michigan Lobe fluctuations during the last glacial maximum. Quat. Res. 89, 739–755.
- NCL, 2018. The NCAR Command Language [Software], 6.5.0. UCAR/NCAR/CISL/TDD, Boulder, CO.
- Oster, J.L., Ibarra, D.E., Winnick, M.J., Maher, K., 2015. Steering of westerly storms

- over western north America at the last glacial maximum. Nat. Geosci. 8, 201–205
- Otvos, E.G., 2004. Prospects for interregional correlations using Wisconsin and Holocene aridity episodes, northern Gulf of Mexico coastal plain. Quat. Res. 61, 105–118
- Pausata, F.S.R., Li, C., Wettstein, J., Kageyama, M., Nisancioglu, K.H., 2011. The key role of topography in altering North Atlantic atmospheric circulation during the last glacial period. Clim. Past 7, 1089—1101.
- Pausata, F.S.R., Li, C., Wettstein, J., Nisancioglu, K.H., Battisti, D.S., 2009. Changes in atmospheric variability in a glacial climate and the impacts on proxy data: a model intercomparison. Clim. Past 5.
- Peltier, W.R., 2004. Global glacial isostacy and the surface of the ice age earth: the ICE-5G (VM2) Model and GRACE. Annu. Rev. Earth Planet Sci. 32, 111–149.
- Pigati, J.S., McGeehin, J.P., Muhs, D.R., Grimley, D.A., Nekola, J.C., 2015. Radiocarbon dating loess deposits in the Mississippi Valley using terrestrial gastropod shells (Polygyridae, Helicinidae, and Discidae). Aeolian Research 16, 25–33.
- Rodbell, D.T., Forman, S.L., Pierson, J., Lynn, W.C., 1997. Stratigraphy and chronology of Mississippi Valley loess in western Tennessee. Geol. Soc. Am. Bull. 109, 1134–1148
- Roderick, M.L., Rotstayn, L.D., Farquhar, G.D., Hobbins, M.T., 2007. On the attribution of changing pan evaporation. Geophys. Res. Lett. 34.
- Roe, G., 2009. On the interpretation of Chinese loess as a paleoclimate indicator. Ouat. Res. 71, 150–161.
- Ruhe, R.V., 1954. Relations of the properties of Wisconsin loess to topography in western Iowa. Am. J. Sci. 252, 663–672.
- Rutledge, E.M., Holowaychuk, N., Hall, G.F., Wilding, L.P., 1975. Loess in Ohio in relation to several possible source areas: I. Physical and chemical properties. Soil Sci. Soc. Am. Proc. 39, 1125–1132.
- Scheff, J., Frierson, D.M.W., 2012. Robust future precipitation declines in CMIP5 largely reflect the poleward expansion of model subtropical dry zones. Geophys. Res. Lett. 39.
- Smith, G.D., 1942. Illinois Loess: Variations in its Properties and Distribution, a Pedologic Interpretation, vol. 490. University of Illinois Agricultural Experiment Station Bulletin, pp. 139–184.
- Soden, B.J., Vecchi, G.Â., 2011. The vertical distribution of cloud feedback in coupled ocean-atmosphere models. Geophys. Res. Lett. 38.
- Snowden, J.O., Priddy, R.R., 1968. Geology of Mississippi loess. Mississippi Geol. Surv. Bull. 111, 13–203.
- St George, S., Wolfe, S.A., 2009. El Niño stills winter winds across the southern Canadian Prairies. Geophys. Res. Lett. 36.
- Sweeney, M., Etyemezian, V., Macpherson, T., Nickling, W., Gillies, J., Nikolich, G., McDonald, E., 2008. Comparison of PI-SWERL with dust emission measurements from a straight-line field wind tunnel. J. Geophys. Res.: Earth Surf. 113.
- Sweeney, M.R., Mason, J.A., 2013. Mechanisms of dust emission from Pleistocene loess deposits, Nebraska, USA. J. Geophys. Res. Earth Surf. 118, 1460–1471.
- Swineford, A., Frye, J.C., 1951. Petrography of the Peoria loess in Kansas. J. Geol. 59, 306–322.
- Ullman, D.J., LeGrande, A.N., Carlson, A.E., Anslow, F.S., Licciardi, J.M., 2014. Assessing the impact of Laurentide Ice Sheet topography on glacial climate. Clim. Past 10, 487–507.
- Wang, N., Jiang, D., Lang, X., 2018. Northern westerlies during the last glacial maximum: results from CMIP5 simulations. J. Clim. 31, 1135–1153.
- Yim, B.Y., Min, H.S., Kug, J.S., 2016. Inter-model diversity in jet stream changes and its relation to Arctic climate in CMIP5. Clim. Dyn. 47, 235–248.
- Zelinka, M.D., Zhou, C., Klein, S.A., 2016. Insights from a refined decomposition of cloud feedbacks. Geophys. Res. Lett. 43, 9259–9269.